THE JOURNAL OF BIOLOGICAL CHEMISTRY VOL. 289, NO. 14, pp. 9983–9997, April 4, 2014

Annexin A2 Mediates Apical Trafficking of Renal Na^+-K^+-$2Cl^-$ Cotransporter*

Received for publication, December 9, 2013, and in revised form, February 5, 2014 Published, JBC Papers in Press, February 13, 2014, DOI 10.1074/jbc.M113.540948

Christin Dathe[‡], Anna-Lena Daigeler[‡], Wenke Seifert[‡], Vera Jankowski[§], Ralf Mrowka[¶], Ronny Kalis[‖], Erich Wanker[‖], Kerim Mutig[‡], Sebastian Bachmann[‡1], and Alexander Paliege[‡2]

From the [‡]Department of Anatomy, Charité-Universitätsmedizin Berlin, 10115 Berlin, the [§]Department of Nephrology, Charité-Universitätsmedizin Berlin, 12203 Berlin, [¶]Experimental Nephrology, Klinik für Innere Medizin III, Universitätsklinikum Jena, 07749 Jena, and [‖]Neuroproteomics, Max Delbrück Center for Molecular Medicine, 13125 Berlin, Germany

Background: Regulated membrane expression of the renal furosemide-sensitive Na^+-K^+-$2Cl^-$ cotransporter (NKCC2) determines essential functions of the kidney.
Results: Annexin A2 (AnxA2) is a new interaction partner of NKCC2 with respect to its adluminal trafficking and activation.
Conclusion: Discussion focuses on trafficking, membrane association, and phosphorylation of NKCC2 and its cellular ligand AnxA2.
Significance: AnxA2 is relevant for the activation of NKCC2.

The furosemide-sensitive Na^+-K^+-$2Cl^-$ cotransporter (NKCC2) is responsible for urine concentration and helps maintain systemic salt homeostasis. Its activity depends on trafficking to, and insertion into, the apical membrane, as well as on phosphorylation of conserved N-terminal serine and threonine residues. Vasopressin (AVP) signaling via PKA and other kinases activates NKCC2. Association of NKCC2 with lipid rafts facilitates its AVP-induced apical translocation and activation at the surface. Lipid raft microdomains typically serve as platforms for membrane proteins to facilitate their interactions with other proteins, but little is known about partners that interact with NKCC2. Yeast two-hybrid screening identified an interaction between NKCC2 and the cytosolic protein, annexin A2 (AnxA2). Annexins mediate lipid raft-dependent trafficking of transmembrane proteins, including the AVP-regulated water channel, aquaporin 2. Here, we demonstrate that AnxA2, which binds to phospholipids in a Ca^{2+}-dependent manner and may organize microdomains, is codistributed with NKCC2 to promote its apical translocation in response to AVP stimulation and low chloride hypotonic stress. NKCC2 and AnxA2 interact in a phosphorylation-dependent manner. Phosphomimetic AnxA2 carrying a mutant phosphoacceptor (AnxA2-Y24D-GFP) enhanced surface expression and raft association of NKCC2 by 5-fold upon low chloride hypotonic stimulation, whereas AnxA2-Y24A-GFP and PKC-dependent AnxA2-S26D-GFP did not. As the AnxA2 effect involved only non-phosphorylated NKCC2, it appears to affect NKCC2 trafficking. Overexpression or knockdown experiments further supported the role of AnxA2 in the apical translocation and surface expression of NKCC2. In summary, this study identifies AnxA2 as a lipid raft-associated trafficking factor for NKCC2 and provides mechanistic insight into the regulation of this essential cotransporter.

The renal furosemide-sensitive Na^+-K^+-$2Cl^-$ cotransporter (NKCC2)[3] resides in the luminal membrane and in apical vesicles of thick ascending limb (TAL) cells and mediates transcellular reabsorption of ~30% of the filtered NaCl load (1–3). Loss-of-function mutations of NKCC2 lead to the antenatal form of Bartter syndrome with severe salt loss in patients (4, 5). Genetic deletion of the transporter in mice is lethal due to dramatic salt loss and extracellular volume depletion (6), whereas its overactivity may contribute to hypertension (7). In view of its influence on the urinary concentrating mechanism and systemic salt homeostasis, major efforts have been undertaken in the past to elucidate its regulation (1–3, 8). Several endocrine and paracrine stimuli as well as changes in osmolality may influence surface expression and activity of the cotransporter (3, 8, 9). Vasopressin (AVP) is particularly effective in this respect. It may enhance TAL transport via its binding to the basolateral $G\alpha_s$-coupled V2 receptor, cAMP release, and resultant rapid adjustments of NKCC2 surface expression and function (3, 10, 11). Several functionally relevant phosphoacceptor sites within the N-terminal domains of NKCC2 have been identified. These become phosphorylated upon AVP administration and may, in part, contribute to activating the cotransporter (12–16). At least two independent kinase pathways are involved. One targets the conserved N-terminal threonine residues of NKCC2 by means of multiple interactions of no lysine kinase (WNK) isoforms and two homologous Ste20-related kinases, oxidative

* This work was supported by Grants NGFN/01GR0807 and 13920B from the Federal Ministry of Education and Research and by Grants FP7-HEALTH-2009-2.4.5-2 to "SYSKID" (241544) and "HEALTH 2011.2.4.2-2" to "Mascara" (278249) from the European Union.
[1] To whom correspondence may be addressed. Tel.: 49-030-450528001; Fax: 49-030-540528922; E-mail: sebastian.bachmann@charite.de.
[2] To whom correspondence may be addressed. Tel.: 49-030-450528001; Fax: 49-030-540528922; E-mail: alexander.paliege@charite.de.

[3] The abbreviations used are: NKCC2, Na^+-K^+-$2Cl^-$ cotransporter; AVP, vasopressin; AnxA2, annexin A2; TAL, thick ascending limb; raTAL, rat medullary thick ascending limb; IP, immunoprecipitation; dDAVP, desmopressin; DI, diabetes insipidus; qPCR, quantitative PCR; MD, macula densa; mTAL, medullary kidney TAL; cTAL, cortical TAL; SAGE, serial analysis of gene expression.

stress-responsive kinase 1 (OSR1), and STE20/SPS1-related Pro/Ala-rich kinase (SPAK) (14, 15, 17). The other likely depends on the catalytic activity of protein kinase A (PKA) or AMP-activated protein kinase and targets NKCC2 at a different site (15, 18–20). It is still unclear whether phosphorylation interferes with NKCC2's membrane insertion or retrieval (3).

Once expressed on the cell surface, a major proportion of NKCC2 is found within cholesterol- and glycosphingolipid-enriched membrane microdomains or lipid rafts (21, 22). Partitioning of the cotransporter into lipid rafts appears to interfere with its regulated cellular translocation, including apical trafficking and endocytic retrieval (21–23). Molecular determinants involved in raft-dependent trafficking events have, however, barely been characterized so far.

Annexins have been shown to mediate lipid raft-dependent trafficking of several transmembrane proteins (24–26). Members of the annexin protein family are known to associate with membrane phospholipids and facilitate membrane fusion of cytoplasmic vesicles with the plasma membrane (27–29). One particular member, annexin A2 (AnxA2), has specific roles in the kidney, where it mediates cAMP-induced trafficking of aquaporin 2 in the collecting duct (30). AnxA2 is expressed in TAL as well, where cAMP-induced fusion of NKCC2-carrying vesicles with the luminal plasma membrane permits rapid surface recruitment and activation of apically stored NKCC2 (12, 19, 31–34). We assumed a functional relation between AnxA2 and NKCC2 based on our present yeast two-hybrid assay data. AnxA2 may bind raft lipids to facilitate the clustering of cholesterol and glycosphingolipids and may thereby promote raft formation and support membrane fusion events, *e.g.* apical vesicles carrying the NKCC2 transporter (35). To do so, AnxA2 may act as a monomer or as a heterotetrameric complex together with its binding partner, the S100A10 protein (also termed p11) (27, 36).

Here, we have identified AnxA2 as a component involved in NKCC2 trafficking. AnxA2 directly and selectively interacts with the N-terminal cytoplasmic domain of the cotransporter in its nonphosphorylated state and facilitates the apical translocation of NKCC2 in response to activation of TAL transport capacity by AVP or low chloride hypotonic stimulation.

EXPERIMENTAL PROCEDURES

Animals and Cells—Adult male Sprague-Dawley rats and Brattleboro rats with diabetes insipidus (DI; all rats 10–14 week old) received standard diet and tap water *ad libitum*. DI rats received an intraperitoneal injection of the V2 receptor agonist, 1-*deamino*-8-D-arginine vasopressin (dDAVP; 1 μg/kg body weight), or vehicle (0.9% saline; $n = 8$ rats per group). For histochemical analysis, rats were anesthetized with Nembutal (100 mg/kg body weight); the abdominal cavity opened, and kidneys were fixed by retrograde perfusion through the abdominal aorta using 3% paraformaldehyde in PBS (37). Kidneys were then processed for cryostat and paraffin sectioning. For biochemical studies, rats were anesthetized with isoflurane and killed by cervical dislocation; kidneys were then removed, dissected into cortical and medullary portions, and processed for the biochemical evaluation.

Mouse macula densa-derived 1 cells (MMDD1) (38) were cultured in DMEM/F-12 containing L-glutamine, 10% fetal calf serum (FCS), and 1% penicillin/streptomycin (37 °C, 5% CO_2). Rat medullary thick ascending limb cells (raTAL) (39) were cultured in renal epithelial growth medium (Promo Cell) supplemented with 1% penicillin/streptomycin at 37 °C 5% CO_2. Human embryonic kidney (HEK293) cells were cultured in α-minimal essential medium (Lonza) supplemented with 5% FCS and 2 mM L-glutamine (37 °C, 5% CO_2). Transient transfection experiments were performed using JetPEI (Polyplus transfection) according to the manufacturer's protocol. Low chloride hypotonic stress was induced in MMDD1 cells or raTAL cells by treating them with hypotonic low chloride solution (25 mM $NaHCO_3$, 0.96 mM NaH_2PO_4, 0.24 mM Na_2HPO_4, 5 mM KCl, 1.2 mM $MgSO_4$, 1 mM $CaCl_2$, 5.5 mM glucose) for 1 h; isotonic normal chloride solution was used for control (+100 mM NaCl) (40). For cytochemical analysis, cells were fixed with 3% paraformaldehyde in PBS for 15 min at 4 °C or precooled 100% methanol for 5 min at −20 °C. For biochemical studies, cells were lysed, diluted in 1× Laemmli buffer, and analyzed by immunoblotting.

Immunohistochemistry—Tissue sections were produced from paraffin-embedded or frozen material. Paraffin sections were dewaxed and boiled for 6 min in citrate buffer, pH 6, for antigen retrieval. Fixed cultured cells were treated for 10 min at room temperature with 0.5% Triton X-100, 1% bovine serum albumin (BSA) in PBS. The following general blocking step was performed on tissue sections with 5% skim milk in PBS for 30 min or on cells with 1% BSA in PBS. The respective primary antibodies were applied overnight at 4 °C and rinsed in PBS, and suitable secondary Cy2- or Cy3-conjugated antibodies (Dianova) were then incubated for 1 h. Tissue was then mounted in glycerol/PBS, and coverslips were mounted on glass slides with Fluoromount-G (SouthernBiotech) and viewed in a confocal laser microscope (LSM 5 Exciter, Zeiss).

Tissue Preparation and Fractionation—Renal tissue samples were homogenized in homogenization buffer (250 mM sucrose, 10 mM triethanolamine, and protease inhibitors, pH 7.5) by grinding and subsequent ultrasonication. Cell debris and nuclei were removed by centrifugation at 1,000 × *g* for 15 min at 4 °C. Protein concentrations of the obtained postnuclear lysates were determined by the Bradford method using the BCA-protein assay reagent kit (Pierce). Plasma membrane-enriched fractions were separated by additional centrifugation at 16,000 × *g* for 30 min at 4 °C. The remaining supernatant fraction was thus enriched in cytoplasmic structures and vesicles. 50 μg of protein were loaded per lane for immunoblotting.

Isolation of Lipid Rafts by Triton X-100 and Sucrose Gradient Fractionation—Lipid raft extraction was performed as described previously (41). Briefly, outer medullary postnuclear lysates were centrifuged at 120,000 × *g* for 1 h at 4 °C to obtain membranes and vesicles. The obtained pellets were resuspended in ice-cold homogenization buffer supplemented with 1% Triton X-100 and incubated for 1 h at 4 °C under agitation, followed by ultracentrifugation at 120,000 × *g* for 1 h at 4 °C. The resulting pellets containing the detergent-insoluble fractions were resuspended in 2 ml of homogenization buffer with 40% sucrose and overlaid with 5 ml of 30% sucrose and 5 ml 5%

sucrose to create a discontinuous sucrose gradient required for floating assay. The gradient was centrifuged overnight at 40,000 rpm and 4 °C. Twelve 1-ml fractions were removed from the top of the gradient and analyzed by immunoblotting.

Immunoprecipitation of NKCC2 and AnxA2—NKCC2 and AnxA2 were immunoprecipitated from medullary lysates or lipid raft-enriched fractions of the discontinuous sucrose gradient (see above). Anti-NKCC2 (Millipore) or anti-AnxA2 (Santa Cruz Biotechnology) antibodies were coupled to Dynabeads according to the manufacturer's guidelines (Dynabeads M-270 Epoxy; antibody coupling kit (Invitrogen)). Lipid raft-enriched fractions of the floating assay were identified by the presence of the typical raft proteins such as flotillin-1 and Tamm-Horsfall protein, pooled, and centrifuged at 40,000 × *g*. The resulting pellets were dissolved in immunoprecipitation (IP) buffer (TBS containing 0.5% Tween 20 and proteinase inhibitor). Postnuclear rat outer medullary lysates (10 μg/μl) or lipid raft-enriched extracts (5 μg/μl) were incubated with antibody-coupled beads overnight at 4 °C upon gentle agitation. The beads were washed three times with IP buffer followed by a stringent washing step (300 mM NaCl in IP buffer). Beads were boiled in 1× Laemmli buffer to elute the precipitated proteins, and eluates were analyzed by immunoblotting.

SDS-PAGE and Immunoblotting—For immunoblotting, 30 μg of protein or 20 μl of immunoprecipitates per lane were subjected to 10% SDS-PAGE and transferred to nitrocellulose membranes. The membranes were blocked with 5% skim milk in PBS, incubated with primary antibodies (1 h at room temperature and overnight at 4 °C), washed, incubated with the appropriate HRP-conjugated secondary antibodies (DAKO; 1 h at room temperature), and subjected to chemiluminescence for signal detection (ECL; Amersham Biosciences). Signals were quantified by densitometry.

Antibodies—Immunohistochemistry and immunoblotting steps were performed using the following primary antibodies: anti-NKCC2 (37, 42); anti-NKCC1/2 (T4; Developmental Studies Hybridoma Bank); anti-Tamm-Horsfall protein (43); anti-flotillin-1 (BD Biosciences); anti-transferrin receptor (Santa Cruz Biotechnology); anti-clathrin (BD Biosciences); anti-transferrin receptor (Santa Cruz Biotechnology); anti-AnxA2 (Santa Cruz Biotechnology); anti-phospho-Y24-AnxA2 (Santa Cruz Biotechnology); anti-S100A10 (Acris); anti-GFP (Roche Applied Science); anti-GAPDH (Santa Cruz Biotechnology); anti-α-tubulin (Sigma), and anti-GST (Sigma). Immunoprecipitation experiments were performed using anti-NKCC2 antibody (Millipore) and anti-AnxA2 (Santa Cruz Biotechnology).

Yeast Two-hybrid—Yeast two-hybrid screening was performed in an automated interaction-mating-matrix approach as described (44). DNA coding for two overlapping N-terminal fragments (AS(40–140) and AS(77–177)) of human NKCC2 were amplified by PCR using a full-length clone for human NKCC2 as template (DKFZp686O14110Q or IRATp970G1058D (ImaGenes)). For generation of bait plasmids, PCR fragments were cloned into a pBTM117c yeast expression vector to generate fusion proteins containing a LexA binding domain and one of the NKCC2 fragments. As a selection marker, the vector contains the gene for phosphoribosylanthranilate isomerase (*trp1*), an enzyme required for tryptophan biosynthesis (45). Haploid L40ccMATa yeasts were transformed with bait plasmids and subsequently mated to a matrix of 16,888 individual L40ccMATα yeast clones transformed with pACT-4 vectors that code for a set of nonredundant human proteins fused to a GAL4 activation domain and β-isopropylmalate dehydrogenase (Leu2) as a selection marker. Diploid cells were grown on SDII media deficient for tryptophan and leucine to select for the presence of both bait and prey plasmids. Physical interaction of the NKCC2 fragment with the respective prey protein results in the reconstitution of the GAL4 transcription factor that drives the expression of (lexAop)4-HIS3, (lexAop)8-URA3, and β-galactosidase reporter genes and thus allows growth on SDIV selection media lacking tryptophan, leucine, histidine, and uracil. All clones were also screened for their β-galactosidase activity using LacZ staining as described previously (46). To increase the stringency of the assay, the SDIV and LacZ approaches were run in triplicate and evaluated in a blinded fashion. Only clones that grew three times on SDIV medium and were at least positive twice for LacZ were considered valid hits. Identified candidates were subsequently ranked based on their TAL expression. To this end mRNA serial analysis of gene expression (SAGE) tags detected in the human nephron segments were mapped to human coding cDNA sequences. Nephron-specific SAGE tags were obtained as described previously (32, 47). Human cDNA data were obtained from ENSEMBL (48) with the BIOMART tool (49). Using scripting software developed in-house, we mapped the SAGE tags to the cDNA and obtained for each gene a score for the nephron parts as follows: glomerulus; proximal convoluted tubule; proximal straight tubule; medullary thick ascending limb; cortical thick ascending limb; distal convoluted tubule; cortical collecting duct; outer medullary collecting duct, total. The ratio of (MTAL+CTAL)/total was used to indicate TAL-specific expression. A list of genes was produced that indicated positive yeast two-hybrid screening results and a high TAL expression according to the SAGE tag analysis.

Mass Spectrometry—NKCC2 and control IgG immunoprecipitates from lipid raft-enriched outer medullary fractions were subjected to SDS-PAGE and Coomassie Brilliant Blue staining. The bands produced by NKCC2 IP were excised, and the gel plugs were washed and equilibrated with ammonium bicarbonate in acetonitrile and digested with 0.02 μg of trypsin at 37 °C for 24 h. The resulting peptides were desalted and concentrated utilizing the $ZipTip_{C18}$ (Millipore) technology and eluted directly onto the MALDI target (Bruker Daltonik) using α-cyano-4-hydroxycinnamic acid as matrix. The subsequent mass spectrometry (MS) analyses were carried out using a matrix-assisted laser desorption/ionization time-of-flight mass spectrometry (MALDI-TOF MS, MALDI-Lift fragment mass-spectrometry (MALDI-TOF-TOF MS; Bruker)). Calibrated and annotated spectra were subjected to a database search (Swiss-Prot) utilizing the Bruker Bio-Tool 3.2 and the Mascot 2.2 search engine, which compare the experimental MALDI-TOF MS and MALDI-TOF-TOF MS data set with the calculated peptide masses for each entry into the sequence database

TABLE 1

Results of yeast two-hybrid assay

Yeast two-hybrid assay identified 36 candidate proteins as potential interacting partners with N-terminal fragments of NKCC2. Subsequent ranking of the candidates according to their expression in the TAL identifies AnxA2 among the proteins with the highest expression levels. Top hits of positive interacting genes of the yeast two-hybrid screen sorted according to the score indicating the relative TAL expression (last column). This score derives from the cTAL and mTAL SAGE hits. Base count refers to the cDNA length of the transcript. The 2nd column refers to the Ensemble database gene identifier and 3rd and 4th columns to yeast two-hybrid screening results.

Gene symbol	ENSG	SDIV repeat	LacZ repeat	Base count	cTAL + mTAL	(cTAL + mTAL)/base count
ANXA2	ENSG00000182718	3	2	33,299	7,218	0.22
GNL1	ENSG00000229470	3	2	19,612	3,886	0.2
AP2B1	ENSG00000006125	3	3	36,000	4,595	0.13
TLE6	ENSG00000104953	3	2	13,053	1,638	0.13
MAF1	ENSG00000179632	3	2	6,772	845	0.12
MKNK1	ENSG00000079277	3	2	35,399	4,414	0.12
VPS39	ENSG00000166887	3	2	17,646	2,047	0.12
PHTF1	ENSG00000116793	3	2	29,375	3,395	0.12
NDRG4	ENSG00000103034	3	2	62,703	6,654	0.11
HOXC4	ENSG00000198353	3	2	3,768	361	0.1
HAAO	ENSG00000162882	3	3	7,043	665	0.09
MUC7	ENSG00000171195	3	2	9,528	649	0.07

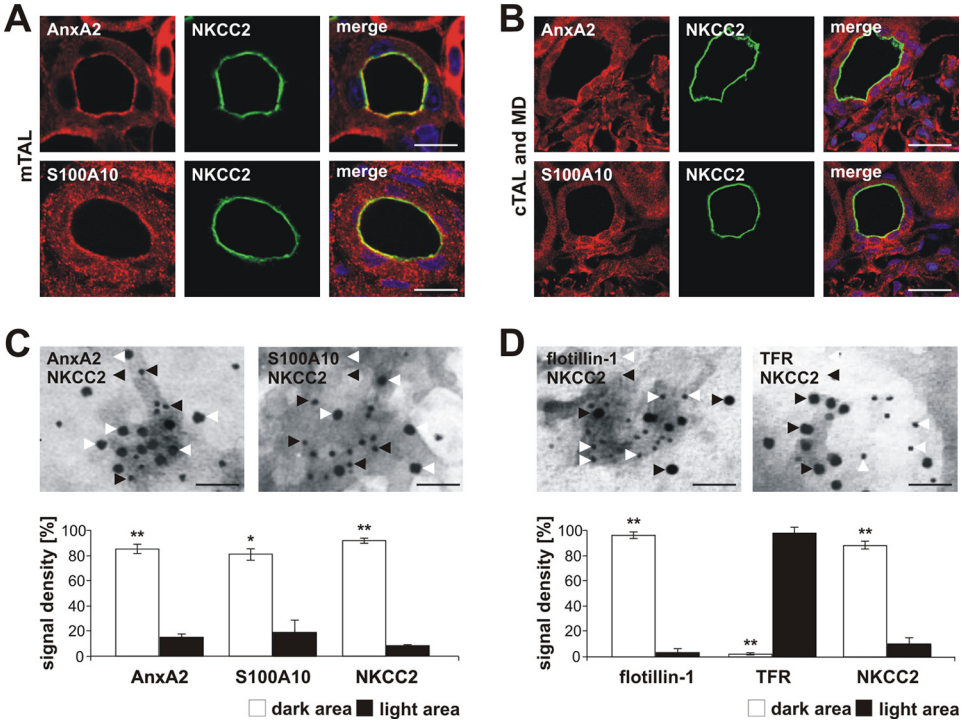

FIGURE 1. **NKCC2 is colocalized with AnxA2 and S100A10 in TAL.** *A* and *B*, confocal images of rat medullary kidney TAL (*mTAL*) and MD double-stained with AnxA2 or S100A10 (*red*) and NKCC2 (*green*). *Merge* images show nuclei counterstained in *blue*; *scale bars*, 20 μm. NKCC2 colocalization with AnxA2 and S100A10 is observed in mTAL. MD also shows colocalization with more cytoplasmic staining of AnxA2 and S100A10 which is absent from cortical TAL (*cTAL*). *C*, cytoplasmic view of luminal plasma membrane sheets from cultured rat TAL cells (*raTAL*) with EM immunogold double labeling of NKCC2 (*black arrows*) and AnxA2 or S100A10 (*white arrowheads*); *scale bars*, 40 nm. All signals are largely restricted to *dark areas*, whereas *light areas* show little signal. Below, quantification of the individual signals is shown. Data are the means ± S.D.; *, $p < 0.05$; **, $p < 0.01$. *D*, same view, with EM immunogold double-labeling of NKCC2 (*black arrowheads*) and flotillin-1 or transferrin receptor (*TFR*; *white arrowheads*); *scale bars*, 40 nm. Although NKCC2 and flotillin-1 signals are colocalized in the dark areas, NKCC2 and transferrin receptor show distinct localization. Below, quantification of the individual signals is shown. Data are the means ± S.D.; *, $p < 0.05$; **, $p < 0.01$.

and use empirically determined factors to assign a statistical weight to each individual peptide match.

DNA Constructs—Full-length mouse AnxA2 (NM_007585.3) and S100A10 (NM_009112.2) were amplified from mouse kidney cDNA using corresponding primer pairs and cloned into pEGFP-N1 or pGEX-6P1 plasmids for transfection experiments or binding assays. The complete N-terminal domain of NKCC2 (coding triplets 1–175; NM_001270617.1) was amplified from rat kidney cDNA and cloned into pGEX-6P1 vector. The mutant NKCC2 N-terminal constructs mimicking constitutive phosphorylation (substitution of Thr or Ser for Asp) or dephosphorylation (substitution of Thr or Ser for Ala) of conserved phosphoacceptor sites (Thr-96, Thr-101, Thr-114, and Ser-126) as well as mutant AnxA2 constructs mimicking constitutive phosphorylation (substitution of Tyr-24 or Ser-26 for Asp) or dephosphorylation (substitution of Tyr-24 for Ala) were generated using site-directed mutagenesis. All constructs were confirmed by sequencing (primer sequences are available on request).

GST Pulldown—After transformation of *Escherichia coli* TOP10 with pGEX-6p1 plasmids containing wild-type or mutant NKCC2 N termini, bacteria were incubated with 0.2 mM isopropyl β-D-thiogalactopyranoside (Thermo Scientific) for 15 h at room temperature to induce protein expression.

After that, bacteria were lysed with lysozyme (Sigma) and Triton X-100. Fusion proteins were purified by overnight incubation of lysates with Glutathione magnetic beads (Pierce) and subsequent washing of beads in pulldown buffer (50 mM HEPES, 200 mM NaCl, 10 mM $CaCl_2$, and protease inhibitors, pH 7.5). HEK293 cells were transfected with wild-type or mutant pEGFP-N1-AnxA2 or pEGFP-N1-S100A10 or pEGFP-N1-AnxA1 and harvested in ice-cold pulldown buffer containing 1% Triton X-100; the resulting HEK293 lysates (10–15 μg/μl) were incubated with GST fusion protein-coupled beads at 4 °C overnight upon agitation. The beads were washed three times with pulldown buffer and boiled once in Laemmli buffer to elute bound proteins, and the eluates were evaluated by immunoblotting.

Peptide Spot Arrays—GST-fused N-terminal tails of wild-type NKCC2 as well as its phosphomimetic or nonphosphomimetic mutants (5 nM) were spotted onto nitrocellulose membranes and incubated with 5% skim milk in TBS adjusted with 1% Tween 20 to block unspecific bindings. After that, wild-type or phospho-AnxA2 mutants (Y24D or S26D) or S100A10 (each 0.1 μM in blocking solution) were applied overnight at 4 °C. Interactions were evaluated by immunoblotting using anti-AnxA2 or anti-S100A10 antibodies. GST was used as negative control, and AnxA2 or S100A10 was spotted on the membrane as positive controls.

Rip/Flip Immunoelectron Microscopy—Preparation of plasma membrane sheets was performed as described (50, 51). Briefly, raTAL cells were grown to confluence on glass coverslips, fixed for 15 min in 0.5% paraformaldehyde/PBS, washed in PBS, and subsequently inverted on glow-discharged nickel electron microscopy grids coated with poly-L-lysine. Gentle pressure was applied to the coverslip for 15 s using a fine pair of forceps. The coverslips were then lifted, leaving portions of the upper cell surface adherent to the poly-L-lysine-coated grid. Membranes were fixed in 2% paraformaldehyde for 20 min at room temperature. Immunogold labeling of AnxA2, S100A10, flotillin-1, or transferrin receptor was performed using the respective primary antibodies and 5- or 10-nm gold-conjugated secondary antibodies (Abcam). For double-labeling of the grids, anti-NKCC2 antibody and 5- or 10-nm gold-conjugated secondary antibody (Abcam) were sequentially applied thereafter. Grids were then fixed in 2% glutaraldehyde in PBS, contrasted in 1% aqueous tannic acid and 1% aqueous uranyl acetate, washed with distilled H_2O, and examined by transmission electron microscopy (EM; Zeiss E905).

RNA Interference—Small interference RNA (siRNA) for AnxA2 (Santa Cruz Biotechnology) or scramble siRNA (negative control) was repeatedly transfected (two transfections with 8-h time intervals) in 40–50% confluent raTAL cells using HiPerFect (Qiagen). After that, cells were grown to confluence for another 50 h. For a rescue experiment, cells were transiently transfected with pEGFP-N1-AnxA2 (JetPEI) and incubated for 24 h. Cells were then lysed for RNA isolation followed by quantitative real time PCR and immunoblotting evaluations.

mRNA Extraction, cDNA Synthesis, and Quantitative PCR (qPCR) Analysis—RNA extraction from cellular or tissue lysates was performed using the TRIzol reagent (Invitrogen) according to the manufacturer's protocol, and cDNA was synthesized by reverse transcription (BioScript, Bioline). qPCR was performed using HOT FIREPol EvaGreen qPCR Mix Plus (Solis BioDyne) and primer pairs specific for AnxA2 (NM_007585.3), NKCC2 (NM_001270618.1), and GAPDH (forward, 5′-tgcaccaccaactgcttagc-3′; reverse, 5′-ggcatggactgtggtcatgag-3′) in the Real Time PCR 7500 system (Applied Biosystems). All samples were determined in triplicate. Threshold cycle (C_t) values were quantified and normalized against GAPDH (ΔC_t), and the calibrator was subtracted ($\Delta\Delta C_t$). Finally, to perform relative quantification, an exponentiation was calculated by use of 2 to the power of $-\Delta\Delta C_t$ (comparative C_t method) (52).

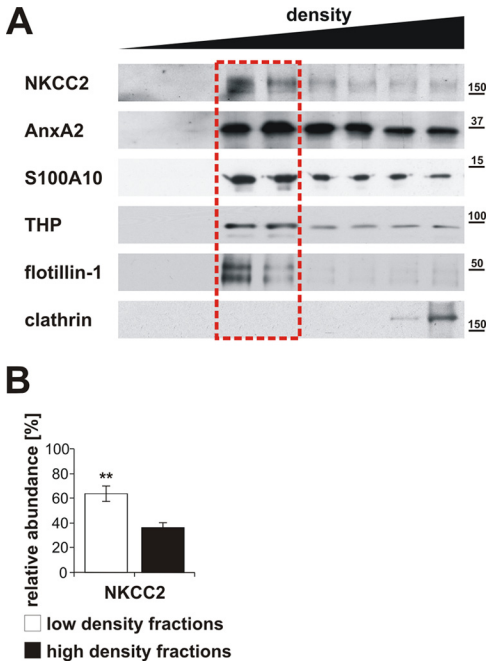

FIGURE 2. **NKCC2 and AnxA2 are substantially codistributed in lipid raft-containing fractions.** *A* and *B*, detergent-resistant membrane rafts were isolated from rat kidney medulla after extraction with Triton X-100 and subsequent sucrose gradient centrifugation. *A*, NKCC2, AnxA2, and S100A10 immunoblot signals showed significant codistribution in the low density fractions (*framed*) along with the raft markers, flotillin-1 and Tamm-Horsfall protein (*THP*). Clathrin serves as a marker for non-raft fractions. *B*, densitometric analysis of the signals in *A*. Data are the means ± S.D.; **, $p < 0.01$.

Analysis of Data—All values are the means ± S.D. Cohorts were compared with Student's two-tailed unpaired *t* test. $p < 0.05$ was accepted as statistically significant.

RESULTS

Identification of AnxA2 as an Interaction Partner of NKCC2 by a Yeast Two-hybrid Screen—To identify candidates that may interact with NKCC2, we first performed yeast two-hybrid screens. Baits consisting of two overlapping N-terminal fragments of human NKCC2 were used to screen a human cDNA library. The choice of the baits was based on the presence of multiply conserved, functionally relevant NKCC2 phosphoacceptor sites (Thr-100, Thr-105, Thr-118, and Ser-130). Yeast two-hybrid screening revealed 36 potential interaction partners of NKCC2 (Table 1). Subsequent ranking of the candidates by their renal expression levels identified AnxA2 as the product with the strongest expression in rat and human TAL. Because annexins may serve as trafficking factors for various transmem-

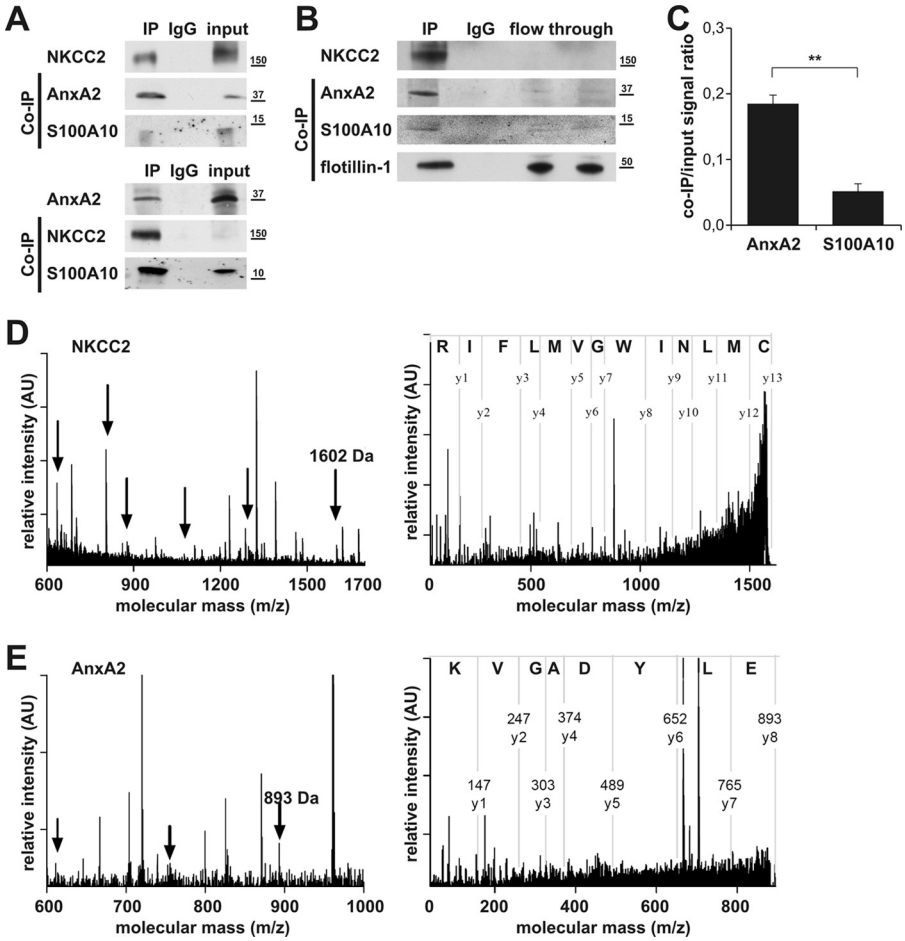

FIGURE 3. **NKCC2 and AnxA2 physically associate in rafts.** *A,* representative immunoblots showing IP of NKCC2 and AnxA2 from medullary rat kidney homogenates. AnxA2 and S100A10 co-IP with NKCC2 as bait, and mutually, NKCC2 and S100A10 co-immunoprecipitate with AnxA2 as bait. IgG indicates control immunoprecipitation with nonspecific IgG. *B,* immunoblots after NKCC2 IP from Triton X-100-insoluble fractions of discontinuous sucrose gradient show co-IP band for AnxA2 and S100A10. Flotillin-1 serves as positive raft marker. *C,* densitometric evaluation of co-immunoprecipitated AnxA2 and S100A10 signals normalized to respective input signals revealed ~3-fold stronger interaction of NKCC2 with AnxA2 as compared with S100A10. Data are the means ± S.D.; **, $p < 0.01$. *D* and *E,* MALDI-TOF mass spectra (*left*) and MALDI-TOF/TOF-MS/MS spectra (*right*) obtained by mass spectrometric evaluation of the eluates after NKCC2 IP from the insoluble gradient fractions confirm the presence of NKCC2 (*D*) and AnxA2 (*E*), supporting their physical association within rafts. *Arrows* point to NKCC2- or AnxA2-specific peptides (*left panels*). *AU,* arbitrary units.

brane proteins (29, 53–55), we hypothesized that AnxA2 may be involved in the trafficking of NKCC2.

Distribution of NKCC2 and AnxA2 in Lipid Rafts—The cellular distribution of AnxA2 was analyzed in rat kidney with a focus on the TAL. Because we have shown before that trafficking of NKCC2 in TAL depends on its distribution in rafts (21), we further analyzed its distribution together with AnxA2 in lipid rafts. There was substantial apical colocalization of AnxA2 with NKCC2 in medullary (m)TAL and macula densa (MD) cells, whereas cortical (c)TAL exhibited weak or no AnxA2 signal by confocal microscopy (Fig. 1, *A* and *B*). S100A10 protein, also termed p11 or AnxA2 light chain, mediates protein interactions with AnxA2 in a scaffolding manner (36, 56, 57). S100A10 was colocalized as well with NKCC2 in mTAL and MD but was absent from cTAL cells (Fig. 1, *A* and *B*). To study whether these components are also colocalized at a high resolution level and whether they are coexpressed within lipid rafts, sheets of the apical membrane were obtained from cultured raTAL cells using the rip/flip technique. We then used EM-immunogold staining of the sheets and confirmed an intimate colocalization of AnxA2 and S100A10 with NKCC2 in dark, electron-dense subdomains. Numerical evaluation confirmed that signals were largely restricted to the dark domains throughout (Fig. 1*C*). To further characterize the distribution of NKCC2 within the dark domains, which have earlier been referred to as rafts (51, 58), double staining with the established raft marker flotillin-1 (59, 60) showed predominant colocalization of the two products in the dark domains, whereas the non-raft protein, transferrin receptor (61, 62), was found outside of the dark domains in the light surroundings, mostly separated from NKCC2 signals. Quantitative evaluation underlined that the majority of NKCC2 signal was restricted to the dark domains likely to represent lipid rafts (Fig. 1*D*). To corroborate these data biochemically, detergent-resistant membrane rafts were isolated from rat kidney medullary homogenate using extraction with Triton X-100 and subsequent sucrose gradient centrifugation. The resulting detergent-insoluble fractions contained NKCC2, AnxA2, and S100A10 as well as flotillin-1 and another raft protein, glycosylphosphatidylinositol-anchored Tamm-Horsfall protein (Fig. 2, *A* and *B*) (63). In aggregate, these data thus support a codistribution of AnxA2, S100A10, and NKCC2 within apical membrane rafts.

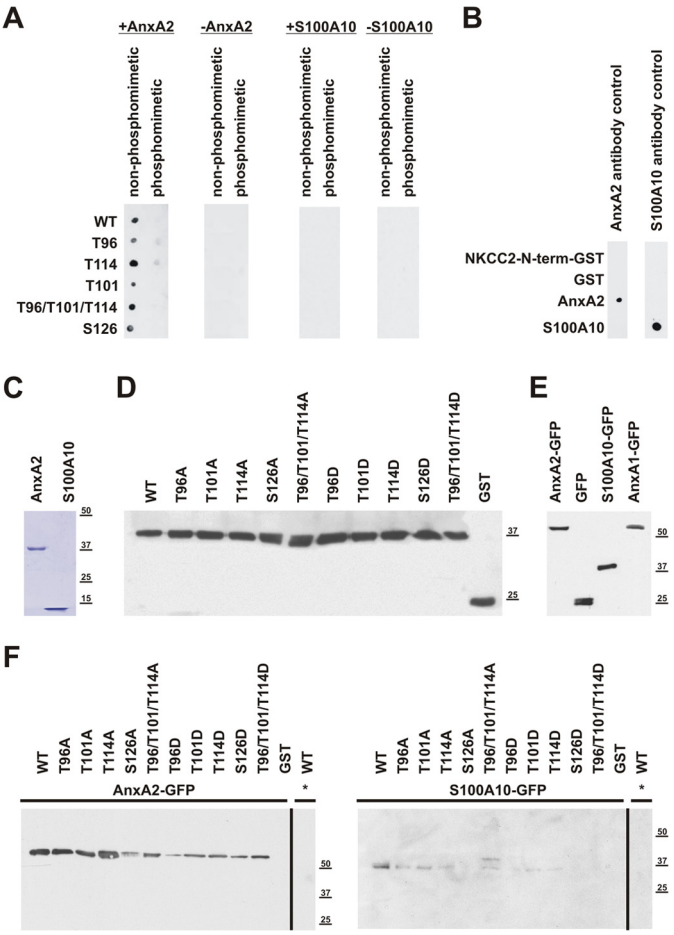

FIGURE 4. **AnxA2 but not S100A10 directly and selectively interact with nonphosphorylated NKCC2 species.** *A,* representative peptide spot assays of interactions between the GST-fused, purified N-terminal tails of wild-type (*WT*) NKCC2 as well as its phosphomimetic or nonphosphomimetic mutants with AnxA2 or S100A10. WT and mutant NKCC2 N termini were spotted to nitrocellulose membranes, incubated with AnxA2 or S100A10, and detected by specific antibodies to AnxA2 or S100A10. AnxA2 selectively binds to WT NKCC2 and the nonphosphomimetic mutants. Note the lack of interactions between WT or mutant NKCC2 N termini and S100A10. *B,* specificity of the assays and the lack of antibody cross-reactivity were tested in control spots. *C,* Coomassie Blue staining of recombinant WT AnxA2 and S100A10. *D,* control immunoblot of GST-fused recombinant WT NKCC2 N terminus and its phosphomimetic and nonphosphomimetic mutants produced in *E. coli*. *E,* control immunoblot showing GFP-tagged AnxA2, S100A10, or AnxA1 produced in HEK293 cells. *F,* immunoblots of eluates after GST pulldown assays using phosphomimetic and nonphosphomimetic NKCC2 mutants as baits and lysates from HEK293 cells transfected with GFP-tagged AnxA2, S100A10, or AnxA1 (*asterisk*). Note strong interactions of AnxA2 with the WT and nonphosphomimetic NKCC2 mutants but less so with the phosphomimetic NKCC2 mutants. NKCC2 N termini show no interaction with S100A10 or AnxA1.

NKCC2 N Terminus Directly Interacts with AnxA2—Rat medullary kidney extracts or derived raft-enriched fractions were used for co-immunoprecipitation (co-IP) experiments to study potential interactions of NKCC2 with AnxA2 or S100A10 (Fig. 3, *A–E*). These experiments revealed substantial physical interaction of NKCC2 with AnxA2 but less so with S100A10 (Fig. 3, *A–C*). To specify interactions at the molecular level, the recombinant N terminus of NKCC2 and the recombinant, complete AnxA2 or S100A10 proteins were studied for interaction using peptide spot assay (Fig. 4, *A–D*). Resulting signals indicated binding between the N terminus of NKCC2 with AnxA2 but not S100A10 (Fig. 4*A*). To specify the role of N-terminal NKCC2 phosphorylation (Thr-96, Thr-101, Thr-114, and Ser-126) in its interaction with AnxA2, phosphomimetic and nonphosphomimetic mutants were tested in spot assays; AnxA2 selectively bound to the nonphosphomimetic mutants (Fig. 4*A*). These data were confirmed by GST pulldown assays using the wild-type and mutant N termini of NKCC2 as baits (Fig. 4, *E* and *F*).

Short Term Administration of Vasopressin Increases Surface Expression and Lipid Raft Association of NKCC2 and AnxA2—AVP is a potent endocrine activator of NKCC2 that promotes its apical trafficking (12, 21, 33). To study the effects of AVP on AnxA2 and S100A10, AVP-deficient Brattleboro rats with central DI were treated with the V2 receptor agonist, desmopressin (dDAVP, 30 min). Immunoblots after tissue fractionation revealed shifts of AnxA2 and NKCC2 by signal increases in the plasma membrane-enriched fractions (+29% for AnxA2 and +28% for NKCC2) compared with decreases in the cytoplasmic fractions (−29% for AnxA2 and −27% for NKCC2; $p < 0.05$); changes of S100A10 were absent (Fig. 5*A*). Confocal evaluation confirmed apical shifting of the AnxA2 signal, whereas the S100A10 signal was practically unaltered. Because of its strictly subapical localization at baseline, a shift of NKCC2 to the surface could not be visualized (Fig. 5*B*). dDAVP further induced parallel shifts of NKCC2 and AnxA2 into the low density sucrose gradient fractions from medullary extracts (+13% for NKCC2 and +19% for AnxA2; $p < 0.05$), suggesting enhanced raft association of both products (Fig. 6*A*). The interaction of NKCC2 with AnxA2 was increased 2-fold in the raft fractions as revealed by co-IP (Fig. 6*B*). Activation of the V2 receptor thus concomitantly stimulated luminal trafficking and raft association of NKCC2 and AnxA2 and corroborated their interaction. Because AnxA2 appears to exclusively interact with nonphosphorylated NKCC2, we suggest that AVP-induced trafficking events precede the phosphorylation of the cotransporter.

AnxA2 Facilitates Membrane Recruitment of NKCC2 upon Low Chloride Hypotonic Stress in Cultured Cells—Low chloride hypotonic stress is an established condition to promote apical trafficking and surface expression of NKCC2 in heterologous models (3, 12, 14, 15). We therefore tested whether under this condition trafficking of endogenous NKCC2 was affected by the presence of AnxA2 or S100A10. To this end, cultured MD cells (MMDD1) were transfected with vectors coding for AnxA2-GFP, S100A10-GFP, or GFP alone and stimulated with low chloride hypotonic stress for 1 h. Cells were then fractionated, and the resulting plasma membrane pool was further extracted with cold detergent. The obtained raft fractions revealed markedly increased signals for NKCC2 upon transfection with AnxA2-GFP (+239%; $p < 0.01$), whereas S100A10-GFP or GFP alone had no effects (Fig. 7, *A* and *B*). The specific role of AnxA2 was further illustrated cytochemically. Upon stimulation, a clear redistribution from the cytosol to the plasma membrane was observed for AnxA2-GFP but less so for S100A10-GFP, and GFP alone showed no effect (Fig. 7*C*). Data therefore suggest that AnxA2 facilitates luminal trafficking and raft association of NKCC2 upon stimulation. To further illustrate the role of AnxA2 in NKCC2 trafficking, AnxA2 deficiency was induced by RNAi-mediated knockdown of its expression. In contrast to MMDD1 cells, which had low endog-

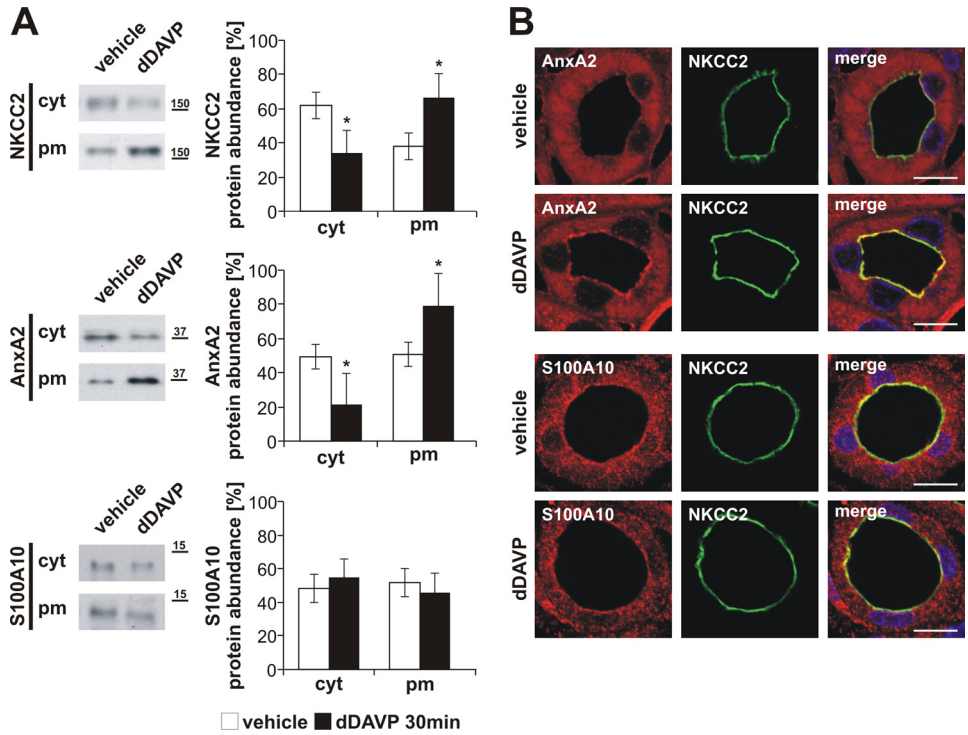

FIGURE 5. **V2 receptor stimulation of rats with diabetes insipidus stimulates trafficking of NKCC2 and AnxA2 but not S100A10.** *A* and *B,* rats were analyzed after 30 min of treatment with desmopressin (dDAVP) or vehicle. *A,* immunoblots of plasma membrane (*pm*)-enriched and cytoplasmic (*cyt*) vesicle containing fractions from medullary kidney homogenates of dDAVP- or vehicle-treated rats. Note significant dDAVP-induced luminal shifts of AnxA2 and additional NKCC2 as reflected by their increased signals in the plasma membrane fractions; signals in cytoplasmic fractions are concomitantly decreased. Distribution of S100A10 signals is unchanged. Data are the means ± S.D.; *, $p < 0.05$. *B,* confocal images show increase of apical AnxA2 signal, whereas S100A10 is unchanged. *Merge* images show nuclei counterstained in *blue*; *scale bars,* 10 μm.

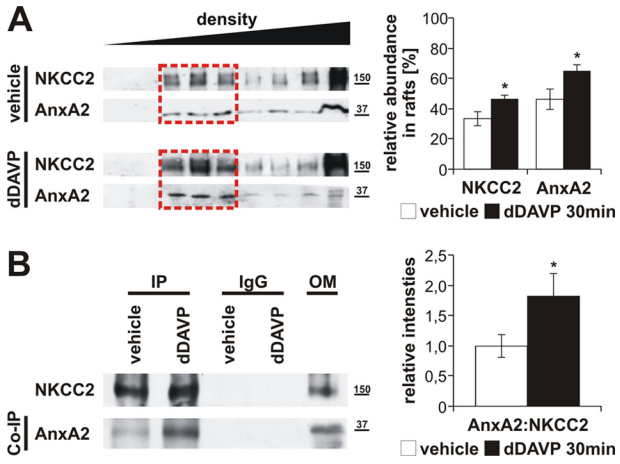

FIGURE 6. **V2 receptor stimulation enhances the interaction between AnxA2 and NKCC2 and corroborates their raft association.** *A,* immunoblots showing distribution of NKCC2 and AnxA2 along discontinuous sucrose gradient from the Triton X-100-insoluble fractions obtained from outer medullary (*OM*) extracts of vehicle- or dDAVP-treated DI rats. Densitometry shows significant shifts from the higher (unframed) to the lower density fractions (*red frames*). *B,* immunoblots showing IP of NKCC2 and co-IP of AnxA2 from the low density fractions. The experiment was controlled by IP using nonspecific IgG. Densitometry of AnxA2-to-NKCC2 signal ratio reflects the strength of their interaction. The data are the means ± S.D.; *, $p < 0.05$.

enous AnxA2 expression, cultured raTAL cells spontaneously displayed substantial abundance of AnxA2 and were therefore more suitable. Transfection with AnxA2 siRNA resulted in a significant knockdown of AnxA2 (−67% at the mRNA level; $p < 0.01$; and −77% at the protein level; $p < 0.01$) after 72 h; the abundance of NKCC2 was unaffected under this condition (Fig. 8, *A* and *B*). Low chloride hypotonic stress for 1 h led to efficient trafficking of NKCC2 to the surface of control cells, whereas in AnxA2-deficient cells, NKCC2 distribution was unchanged (Fig. 8*C*). In addition, control rescue experiments were performed using transient transfection of AnxA2-GFP subsequent to its knockdown. The resulting overexpression of AnxA2-GFP markedly increased AnxA2 abundance and normalized the cellular response to the low chloride hypotonic stress (Fig. 8, *A*–*C*).

AnxA2-NKCC2 Interaction Depends on AnxA2 Phosphorylation—Generally, interactions of AnxA2 with other proteins depend on phosphorylation and/or dephosphorylation at its Tyr-24 residue or at residues Ser-12 and Ser-26 (24, 57, 64–66). We have therefore mutated Tyr-24 to mimic its constitutive phosphorylation (Y24D) or dephosphorylation (Y24A), as well as Ser-26 to mimic its phosphorylation (S26D), and we analyzed these mutants for their ability to interact with NKCC2 in MMDD1 cells. Compared with control GFP transfection, overexpression of AnxA2-Y24D-GFP strongly facilitated surface expression and raft association of NKCC2 in response to low chloride hypotonic stress for 1 h (+510% in Triton-insoluble fractions of plasma membrane; $p < 0.05$), whereas AnxA2-S26D-GFP and AnxA2-Y24A-GFP had only minor effects (Fig. 9, *A* and *B*). Next, interactions between the AnxA2 mutants and the NKCC2 N terminus were analyzed by peptide spot and GST pulldown assays using its phosphomimetic and nonphosphomimetic mutants (Fig. 10, *A*–*E*). As expected, AnxA2-Y24D readily interacted with the WT NKCC2 N terminus and its nonphosphomimetic mutants but not with its phosphomimetic

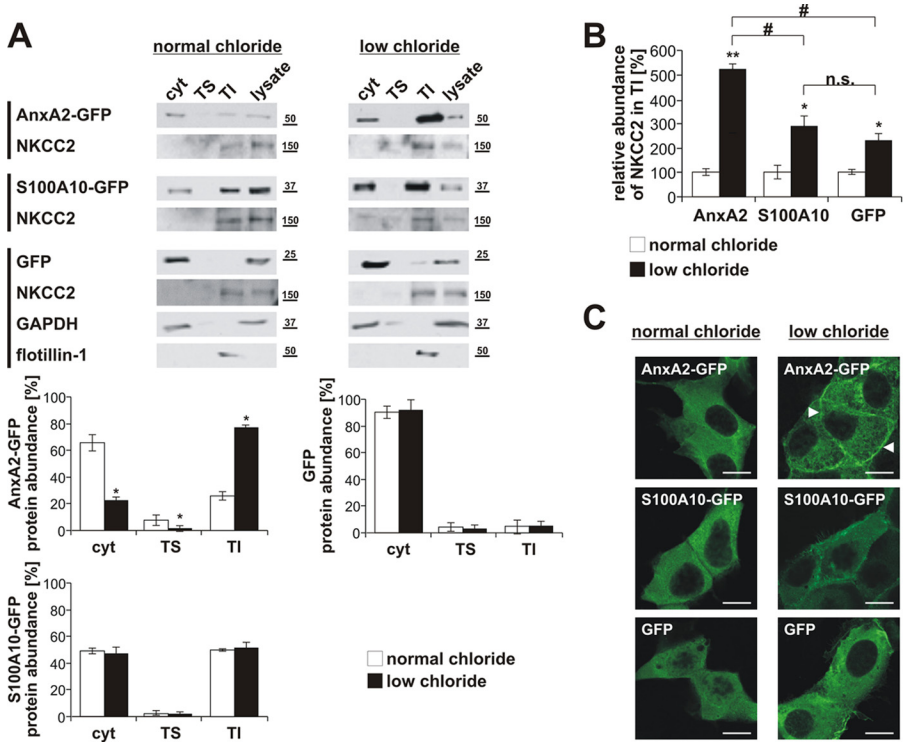

FIGURE 7. **Low chloride hypotonic stress enhances raft association of NKCC2 and AnxA2.** *A,* immunoblots showing cellular distribution of transiently transfected AnxA2-GFP, S100A10-GFP, and GFP and endogenous NKCC2 in MMDD1 cells under normal chloride condition or low chloride hypotonic stress; the cytoplasmic (*cyt*) and the Triton X-100-soluble (*TS*) and -insoluble (*TI*) membrane fractions are shown. Densitometry demonstrates that AnxA2 but not S100A10 or GFP are shifted to the Triton-insoluble fraction. GAPDH was detected as marker of the cytoplasmic fractions, and flotillin-1 was used as a raft marker. Data are the means ± S.D.; *, $p < 0.05$. *B,* densitometric quantification of NKCC2 abundance in the Triton-insoluble membrane fraction from AnxA2-GFP-, S100A10-GFP-, or GFP-transfected cells kept under normal chloride condition or low chloride hypotonic stress. AnxA2-GFP enhances raft association of NKCC2 more than S100A10-GFP or GFP alone. Data are the means ± S.D.; *, $p < 0.05$; **, $p < 0.01$ for differences between low and normal chloride conditions; #, $p < 0.01$ for differences between the transfections. *n.s.,* no significance. *C,* confocal images of the transfected MMDD1 cells under the different chloride conditions. Note increases of plasma membrane-associated AnxA2 (*arrowheads*) but not of S100A10 signals upon low chloride hypotonic stress; *scale bars,* 10 μm.

mutants (Fig. 10, *A* and *D*). In contrast, AnxA2-S26D and AnxA2-Y24A mutants did not exhibit significant interactions either with WT or mutant N-terminal tails of NKCC2 (Fig. 10, *B* and *D*). These results were corroborated by detection of phosphorylated AnxA2 with an anti-phospho-Tyr-24-AnxA2 antibody (pY24-AnxA2) in eluates from GST pulldown assays with rat kidney medulla lysates. Here, the WT NKCC2 N terminus, as well as the mutants mimicking its dephosphorylation, bound the phosphorylated AnxA2, whereas no interactions between the pY24-AnxA2 and the NKCC2 phosphomimetic mutants were detected (Fig. 10*F*). Overall, these results suggest that phosphorylation of AnxA2 at its Tyr-24 residue promotes its interaction with dephosphorylated NKCC2, which in turn facilitates the apical trafficking of the transporter.

DISCUSSION

Activity of a cell membrane transporter or channel, such as NKCC2, principally depends on its surface expression. Our previous work has shown that the distribution of NKCC2 in apical lipid rafts facilitates its anterograde trafficking to the cell surface (21). A role for lipid rafts during endocytic retrieval of NKCC2 has been suggested as well (22); because clathrin, otherwise relevant for its endocytosis, is not a raft-associated protein, this process appears to require uncoupling of at least a proportion of the cell membrane's NKCC2 pool from clathrin (67). Partitioning of NKCC2 to rafts thus appears to substantially determine steps of its surface expression and membrane half-life (21, 23). The detailed impact of NKCC2's raftophilicity in the context of its cellular trafficking was, however, little understood. A potential key to better understand this lies in the fact that lipid rafts may as well serve as scaffolding platforms to facilitate interactions of NKCC2 with other proteins involved in its trafficking (21, 23). Here, we have established AnxA2 as a permissive element in the apical trafficking and surface expression of NKCC2, with both products codistributed in lipid rafts. Furthermore, AnxA2 promoted the association of NKCC2 with rafts, which was probably related with the known property of annexins to bind to negatively charged phospholipids, primarily phosphoinositides, and to stabilize lipid rafts (35, 68–70).

Mechanisms of anterograde trafficking of NKCC2 have been addressed previously. In particular, the role of conserved C-terminal motifs of NKCC2 have been elucidated with respect to its apical sorting (71–73). Here we have shown that the N-terminal tail of NKCC2 is relevant for its surface expression as well, and that intact trafficking requires a direct interaction of its N-terminal domain with AnxA2. This domain encloses several conserved, functionally relevant phosphoacceptor sites (13–15). It has been assumed earlier that phosphorylation of the cotransporter may interfere with its surface expression, although it was unclear whether NKCC2 becomes phosphorylated before, by the time of, or after its insertion in the apical membrane (14,

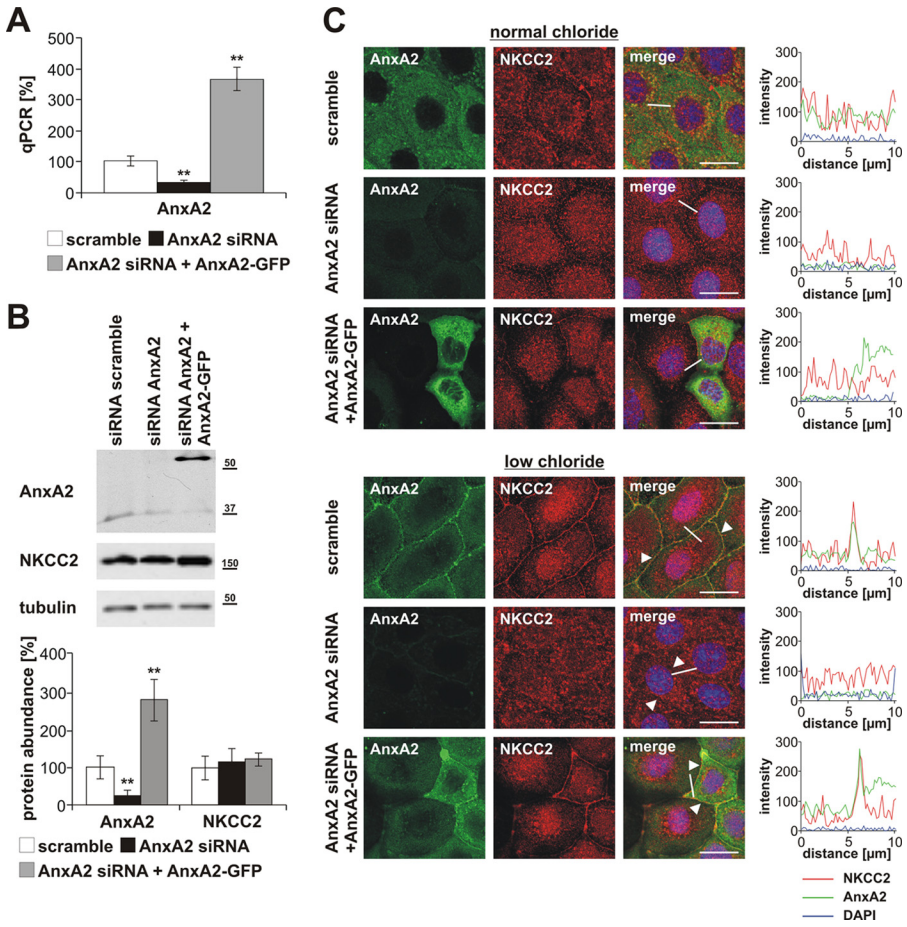

FIGURE 8. **Knockdown of AnxA2 blunts the low chloride hypotonic stress-induced plasma membrane recruitment of NKCC2.** *A–C,* transfections of scramble siRNA (control), AnxA2 siRNA (knockdown), and AnxA2 siRNA with subsequent AnxA2-GFP (rescue) in cultured raTAL cells. *A,* qPCR evaluation. Relative mRNA values were obtained using the comparative C_t method and normalization to GAPDH expression. Data are the means ± S.D.; **, $p < 0.01$. *B,* immunoblots from raTAL cell lysates and densitometric quantification. Note that NKCC2 abundance was generally unaffected. Tubulin serves as loading control; **, $p < 0.01$. *C,* confocal images of transfected raTAL cells kept under normal chloride condition or low chloride hypotonic stress; *scale bars,* 20 μm. Representative confocal profiles of AnxA2 and NKCC2 signal intensities scored across two neighboring cells (*lines*) are shown at the *right* of the corresponding images. Note that the recruitment of NKCC2 into the plasma membrane under low chloride hypotonic stress was blunted after the AnxA2 knockdown but normalized by the rescue of AnxA2 (*arrowheads*).

15). Our present data show that, as far as its interaction with AnxA2 is concerned, trafficking of NKCC2 requires that its N-terminal residues be nonphosphorylated, which implies that NKCC2 membrane insertion precedes its phosphorylation (Fig. 11). This interpretation agrees with the observation that a predominant proportion of phosphorylated NKCC2 is localized in the apical membrane, where it is also colocalizing and interacting with its activating kinases, SPAK and OSR1 (21, 74, 75). The fact that NKCC2 surface expression was unaltered in transgenic mouse models presenting a dramatic decrease or increase of NKCC2 phosphorylation such as SORLA-deficient or SPAK-deficient mice, respectively, further suggests that membrane insertion of the cotransporter does not require its phosphorylation and is thus compatible with AnxA2's permissive role in NKCC2 apical trafficking (74–76).

In the context of raft formation and stabilization, AnxA2 was further proposed to direct cytoplasmic vesicles or domains of organelles to the cytoskeleton to prepare for or to permit their intracellular translocation (69, 77, 78). The present fine structural analysis demonstrates colocalization of AnxA2 and NKCC2 within the same membrane microdomains that were identified as lipid rafts. Along with the additional biochemical evidence of their codistribution in lipid rafts and the evidence of their physical interaction, a role for AnxA2 may as well be suggested in NKCC2 vesicular trafficking. In this respect, cellular translocation of several other transmembrane proteins, including ion transporters and signaling receptors, has been shown to depend on the availability of or the interaction with AnxA2 (24, 25, 79–81). In particular, AnxA2 was shown to determine cAMP-induced trafficking of aquaporin 2 (30). Because both aquaporin 2 and NKCC2 are major targets of AVP (3, 11, 82, 83), AnxA2 appears to have a significant impact in AVP signaling in the two segments harboring these products, TAL and collecting duct, thereby serving to promote urine concentration. The observed AVP-induced stimulation of the interaction intensity between AnxA2 and NKCC2 as well as the pronounced apical shift of AnxA2 upon administration of the extrinsic AVP agonist dDAVP in AVP-deficient DI rats has provided additional supporting evidence for this hypothesis (Fig. 11). Because AnxA2 may be functional in its monomeric form or as a heterotetrameric complex together with its binding partner, protein S100A10, we have tested whether protein S100A10

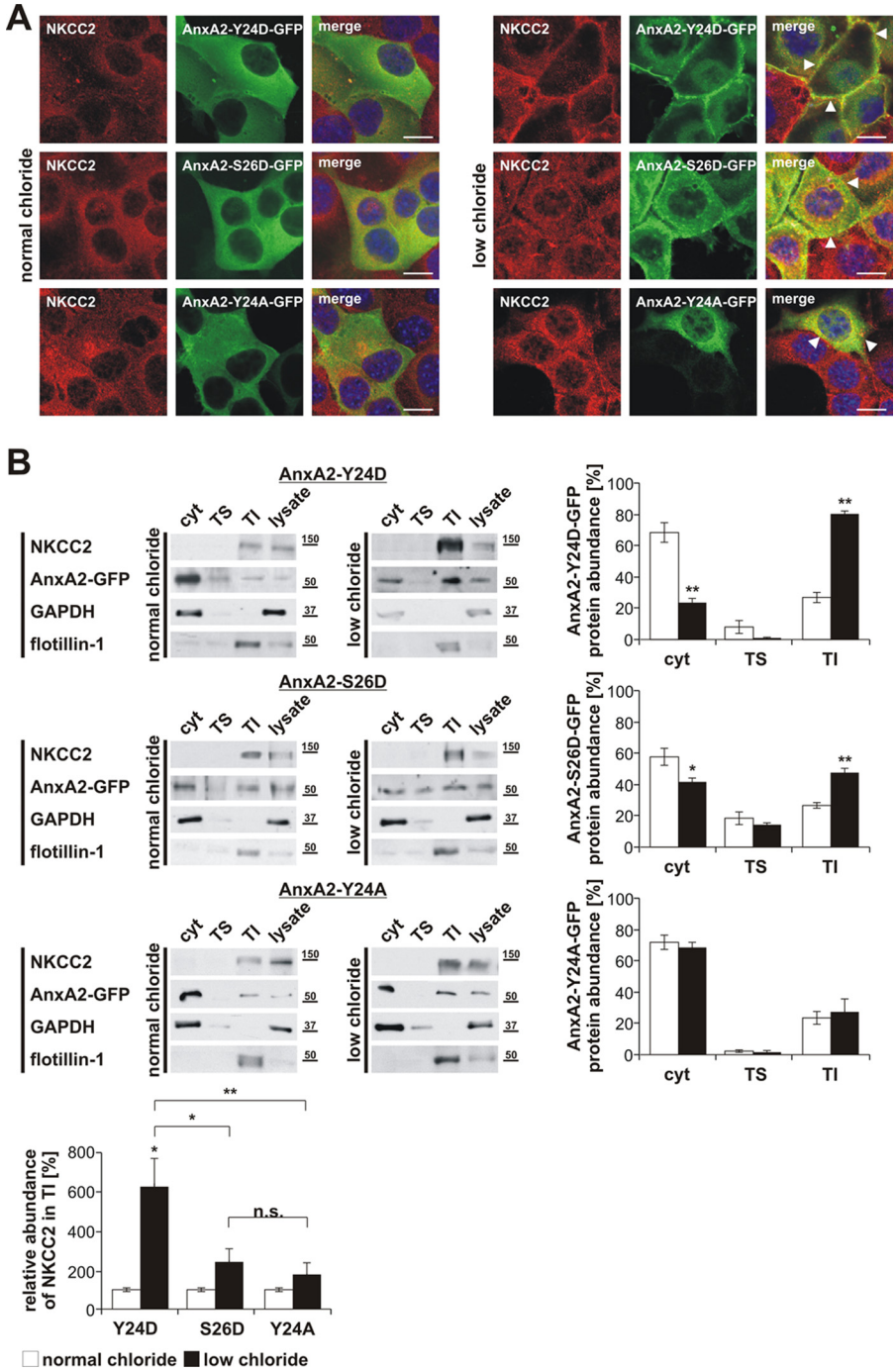

FIGURE 9. **Effects of differential AnxA2 phosphorylation on NKCC2 plasma membrane recruitment and lipid raft association in response to low chloride hypotonic stress.** *A,* confocal images of MMDD1 cells transiently transfected with GFP-tagged AnxA2 mutants mimicking phosphorylation (Y24D or S26D) as well as dephosphorylation (Y24A) following normal chloride condition or low chloride hypotonic stress. AnxA2-Y24D but not AnxA2-S26D or AnxA2-Y24A substantially facilitates plasma membrane recruitment of NKCC2 upon low chloride hypotonic stress. *B,* immunoblots showing abundances of AnxA2-Y24D, AnxA2-S26D, AnxA2-Y24A, and endogenous NKCC2 in cytoplasmic (*cyt*) fractions and Triton-soluble (*TS*) and Triton-insoluble (*TI*) plasma membrane fractions obtained from lysates of MMDD1 cells subjected to normal chloride condition or low chloride hypotonic stress. Densitometric quantification of AnxA2-Y24D, AnxA2-S26D, and AnxA2-Y24A (all fractions) and NKCC2 signals (Triton-insoluble fractions); the data are the means ± S.D.; *, $p < 0.05$; **, $p < 0.01$, *n.s.,* no significance. There is a selective, stronger association of AnxA2-Y24D and NKCC2 with the Triton-insoluble fractions upon low chloride hypotonic stress.

plays a role in the present context as well. Our binding assays demonstrated that, despite the co-distribution of AnxA2, protein S100A10, and NKCC2 in lipid rafts, the interaction between AnxA2 and NKCC2 did not require the presence of protein S100A10. Whereas the physical interaction between AnxA2 and NKCC2 may facilitate trafficking and partitioning to rafts, the tetrameric form of AnxA2 may be functional in stabilizing apical rafts in TAL with the help of protein S100A10 (35, 69, 70, 84, 85).

The N-terminal tail of AnxA2 is a substrate for PKC- and PKA-induced phosphorylation and dephosphorylation events (24, 57, 64, 65). Our data indicate that AnxA2 phosphorylation at Tyr-24 facilitates its interaction with NKCC2, whereas PKC-induced AnxA2 phosphorylation at Ser-26 rather abolishes

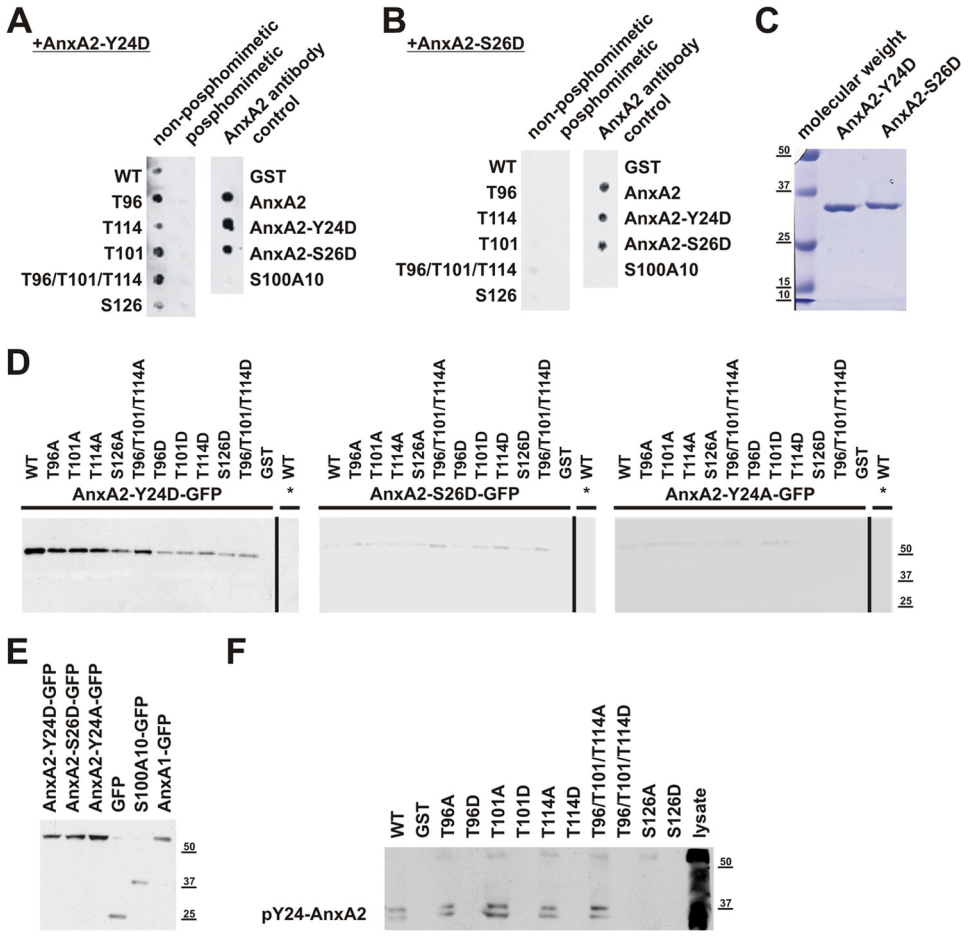

FIGURE 10. **Tyr-24 phosphorylation of AnxA2 promotes its direct interaction with NKCC2.** *A* and *B,* peptide spot assays of interactions between the GST-fused, purified N-terminal phosphomimetic or nonphosphomimetic NKCC2 mutants and AnxA2 mutants mimicking its phosphorylation (Y24D or S26D). NKCC2 mutants were spotted to nitrocellulose membranes, incubated with AnxA2-Y24D (*A*) or AnxA2-S26D (*B*), and detected by anti-AnxA2 antibody. Specificity of the assays and lack of antibody cross-reactivity were verified by detection of the control spots using anti-AnxA2 antibody. *A,* note that the AnxA2-Y24D mutant selectively binds to the nonphosphomimetic NKCC2 mutants. *B,* AnxA2-S26D shows no interactions with either mutant of NKCC2. *C,* Coomassie Blue staining of recombinant AnxA2-Y24D and AnxA2-S26D. *D,* immunoblots of eluates after GST pulldown assays using WT N terminus of NKCC2 and its phosphomimetic and nonphosphomimetic mutants as baits and lysates from HEK293 cells transfected with either GFP-tagged AnxA2-Y24D, AnxA2-S26D, AnxA2-Y24A, or AnxA1 (*asterisk*). There are strong interactions of AnxA2-Y24D with the WT and nonphosphomimetic NKCC2 mutants but less so with the phosphomimetic mutants. AnxA2-S26D and AnxA2-Y24A mutants show only weak interactions with either NKCC2 mutant, whereas AnxA1 does not interact with NKCC2 N termini in this setting. *E,* control immunoblot showing GFP-tagged AnxA2 mutants (Y24D, S26D, and Y24A), S100A10, or AnxA1 produced in HEK293 cells. *F,* GST pulldown assay with NKCC2 N-terminal mutants and lysates from rat kidney medulla showing strong interactions of pY24-AnxA2 with WT NKCC2 N terminus and its nonphosphomimetic mutants but not with the phosphomimetic mutants.

binding of AnxA2 to the transporter. PKA is known to act upstream of calcineurin and thus mediates dephosphorylation of AnxA2 at Ser-26 whereby phosphorylation at Tyr-24 could be promoted (57, 86–88). These results are in line with previously described stimulatory effects of PKA activation on the luminal trafficking of NKCC2 (19, 89). It has been shown that PKA mediates effects of AVP by promoting the anterograde trafficking, as well as recycling of NKCC2 thus increasing its surface expression and activity (3, 10, 11). However, the components operating downstream of the PKA effects have not been elucidated so far (3). Here, we show that the AnxA2 mutant mimicking AnxA2 phosphorylation at Tyr-24 strongly facilitates membrane insertion of NKCC2 upon low chloride hypotonic stress, whereas the AnxA2 mutants mimicking Tyr-24 dephosphorylation or PKC-induced Ser-26 phosphorylation have no stimulatory effects on NKCC2 surface expression. It is therefore tempting to speculate that AnxA2 participates in stimulated apical trafficking/recycling of NKCC2 downstream of PKA activation. Thus, our data provide several lines of evidence that AnxA2 is involved in stimulated NKCC2 trafficking. At the same time, our AnxA2 knockdown or overexpression experiments induced only moderate changes of steady state NKCC2 surface expression suggesting that AnxA2 is not necessary for baseline NKCC2 function but plays a role in the rapid membrane recruitment of the transporter upon stimulation.

Acute increase of NKCC2 surface expression upon appropriate stimulation by AVP or low chloride may involve several synergistic mechanisms such as promotion of anterograde NKCC2 trafficking, rapid membrane insertion of NKCC2-containing vesicles from the apical pool, stimulation of NKCC2 recycling, and probably also inhibition of NKCC2 endocytosis (3, 8, 9). It is currently unclear which one of these processes depends on AnxA2; however, based on its apical distribution in TAL cells, its proposed PKA sensitivity, and its known ability to facilitate the fusion of intracellular vesicles with the

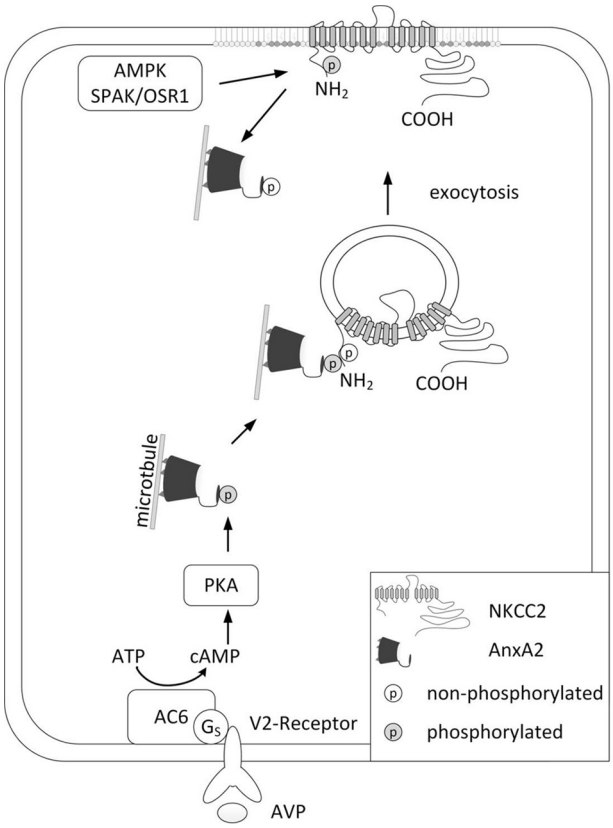

FIGURE 11. **Schematic diagram of AnxA2 function in TAL.** AVP or other cAMP-generating stimuli stimulate Tyr-24 phosphorylation of AnxA2 possibly via the PKA pathway. The phosphorylated AnxA2 selectively binds to the nonphosphorylated N terminus of NKCC2 and promotes its apical trafficking. Exocytotic insertion of NKCC2 into the apical membrane is followed by AnxA2 dissociation and eventual phosphorylation of the transporter at its PKA/AMP-activated protein kinase (*AMPK*)- and SPAK/OSR1-dependent phosphoacceptors.

plasma membrane (24, 57, 64, 66, 77), it may be assumed that AnxA2 is involved in the rapidly occurring membrane insertion events of apical cytoplasmic vesicles containing NKCC2 (Fig. 11).

In summary, we have identified AnxA2 as a novel factor for NKCC2 trafficking that facilitates surface expression of the cotransporter upon stimulation by AVP or low chloride hypotonic stress. While AVP is a major NKCC2 activating hormone, low chloride hypotonic stress leads to a decrease in luminal salt load as it may occur in TAL during physiologic fluctuations or pathophysiologic perturbations. We therefore believe that AnxA2 is involved in the dynamic adjustment of TAL transport function in response to endocrine stimuli or changes in luminal chloride load.

Acknowledgments—We thank Takuya Yamane for providing us with AnxA2 antibody; Nicholas Ferreri for supplying us with cultured rat TAL cells; Henriette Kaminski for technical help, and Kerstin Riskowski and Elisabeth Schindler for excellent technical assistance.

REFERENCES

1. Russell, J. M. (2000) Sodium-potassium-chloride cotransport. *Physiol. Rev.* **80,** 211–276
2. Gamba, G. (2005) Molecular physiology and pathophysiology of electroneutral cation-chloride cotransporters. *Physiol. Rev.* **85,** 423–493
3. Ares, G. R., Caceres, P. S., and Ortiz, P. A. (2011) Molecular regulation of NKCC2 in the thick ascending limb. *Am. J. Physiol. Renal Physiol.* **301,** F1143–F1159
4. Simon, D. B., Karet, F. E., Hamdan, J. M., DiPietro, A., Sanjad, S. A., and Lifton, R. P. (1996) Bartter's syndrome, hypokalaemic alkalosis with hypercalciuria, is caused by mutations in the Na-K-2Cl cotransporter NKCC2. *Nat. Genet.* **13,** 183–188
5. Starremans, P. G., Kersten, F. F., Knoers, N. V., van den Heuvel, L. P., and Bindels, R. J. (2003) Mutations in the human Na-K-2Cl cotransporter (NKCC2) identified in Bartter syndrome type I consistently result in nonfunctional transporters. *J. Am. Soc. Nephrol.* **14,** 1419–1426
6. Takahashi, N., Chernavvsky, D. R., Gomez, R. A., Igarashi, P., Gitelman, H. J., and Smithies, O. (2000) Uncompensated polyuria in a mouse model of Bartter's syndrome. *Proc. Natl. Acad. Sci. U.S.A.* **97,** 5434–5439
7. Chu, P. Y., Cheng, C. J., Wu, Y. C., Fang, Y. W., Chau, T., Uchida, S., Sasaki, S., Yang, S. S., and Lin, S. H. (2013) SPAK deficiency corrects pseudohypoaldosteronism II caused by WNK4 mutation. *PLoS One* **8,** e72969
8. Giménez, I. (2006) Molecular mechanisms and regulation of furosemide-sensitive Na-K-Cl cotransporters. *Curr. Opin. Nephrol. Hypertens.* **15,** 517–523
9. Mount, D. B. (2006) Membrane trafficking and the regulation of NKCC2. *Am. J. Physiol. Renal Physiol.* **290,** F606–F607
10. Knepper, M. A., Kim, G. H., Fernández-Llama, P., and Ecelbarger, C. A. (1999) Regulation of thick ascending limb transport by vasopressin. *J. Am. Soc. Nephrol.* **10,** 628–634
11. Ecelbarger, C. A., Kim, G. H., Wade, J. B., and Knepper, M. A. (2001) Regulation of the abundance of renal sodium transporters and channels by vasopressin. *Exp. Neurol.* **171,** 227–234
12. Giménez, I., and Forbush, B. (2003) Short-term stimulation of the renal Na-K-Cl cotransporter (NKCC2) by vasopressin involves phosphorylation and membrane translocation of the protein. *J. Biol. Chem.* **278,** 26946–26951
13. Giménez, I., and Forbush, B. (2005) Regulatory phosphorylation sites in the NH_2 terminus of the renal Na-K-Cl cotransporter (NKCC2). *Am. J. Physiol. Renal Physiol.* **289,** F1341–F1345
14. Ponce-Coria, J., San-Cristobal, P., Kahle, K. T., Vazquez, N., Pacheco-Alvarez, D., de Los Heros, P., Juárez, P., Muñoz, E., Michel, G., Bobadilla, N. A., Gimenez, I., Lifton, R. P., Hebert, S. C., and Gamba, G. (2008) Regulation of NKCC2 by a chloride-sensing mechanism involving the WNK3 and SPAK kinases. *Proc. Natl. Acad. Sci. U.S.A.* **105,** 8458–8463
15. Richardson, C., Sakamoto, K., de los Heros, P., Deak, M., Campbell, D. G., Prescott, A. R., and Alessi, D. R. (2011) Regulation of the NKCC2 ion cotransporter by SPAK-OSR1-dependent and -independent pathways. *J. Cell Sci.* **124,** 789–800
16. Rieg, T., Tang, T., Uchida, S., Hammond, H. K., Fenton, R. A., and Vallon, V. (2013) Adenylyl cyclase 6 enhances NKCC2 expression and mediates vasopressin-induced phosphorylation of NKCC2 and NCC. *Am. J. Pathol.* **182,** 96–106
17. Moriguchi, T., Urushiyama, S., Hisamoto, N., Iemura, S., Uchida, S., Natsume, T., Matsumoto, K., and Shibuya, H. (2005) WNK1 regulates phosphorylation of cation-chloride-coupled cotransporters via the STE20-related kinases, SPAK and OSR1. *J. Biol. Chem.* **280,** 42685–42693
18. Fraser, S. A., Gimenez, I., Cook, N., Jennings, I., Katerelos, M., Katsis, F., Levidiotis, V., Kemp, B. E., and Power, D. A. (2007) Regulation of the renal-specific Na^+-K^+-$2Cl^-$ co-transporter NKCC2 by AMP-activated protein kinase (AMPK). *Biochem. J.* **405,** 85–93
19. Caceres, P. S., Ares, G. R., and Ortiz, P. A. (2009) cAMP stimulates apical exocytosis of the renal Na^+-K^+-$2Cl^-$ cotransporter NKCC2 in the thick ascending limb: role of protein kinase A. *J. Biol. Chem.* **284,** 24965–24971
20. Gunaratne, R., Braucht, D. W., Rinschen, M. M., Chou, C. L., Hoffert, J. D., Pisitkun, T., and Knepper, M. A. (2010) Quantitative phosphoproteomic analysis reveals cAMP/vasopressin-dependent signaling pathways in native renal thick ascending limb cells. *Proc. Natl. Acad. Sci. U.S.A.* **107,** 15653–15658
21. Welker, P., Böhlick, A., Mutig, K., Salanova, M., Kahl, T., Schlüter, H., Blottner, D., Ponce-Coria, J., Gamba, G., and Bachmann, S. (2008) Renal Na^+-K^+-$2Cl^-$ cotransporter activity and vasopressin-induced trafficking

are lipid raft-dependent. *Am. J. Physiol. Renal Physiol.* **295,** F789–F802
22. Ares, G. R., and Ortiz, P. A. (2012) Dynamin2, clathrin, and lipid rafts mediate endocytosis of the apical Na/K/2Cl cotransporter NKCC2 in thick ascending limbs. *J. Biol. Chem.* **287,** 37824–37834
23. Ares, G. R., and Ortiz, P. A. (2010) Constitutive endocytosis and recycling of NKCC2 in rat thick ascending limbs. *Am. J. Physiol. Renal Physiol.* **299,** F1193–F1202
24. Borthwick, L. A., Neal, A., Hobson, L., Gerke, V., Robson, L., and Muimo, R. (2008) The annexin 2-S100A10 complex and its association with TRPV6 is regulated by cAMP/PKA/CnA in airway and gut epithelia. *Cell Calcium* **44,** 147–157
25. van de Graaf, S. F., Hoenderop, J. G., Gkika, D., Lamers, D., Prenen, J., Rescher, U., Gerke, V., Staub, O., Nilius, B., and Bindels, R. J. (2003) Functional expression of the epithelial Ca^{2+} channels (TRPV5 and TRPV6) requires association of the S100A10-annexin 2 complex. *EMBO J.* **22,** 1478–1487
26. de Graauw, M., Cao, L., Winkel, L., van Miltenburg, M. H., le Devedec, S. E., Klop, M., Yan, K., Pont, C., Rogkoti, V. M., Tijsma, A., Chaudhuri, A., Lalai, R., Price, L., Verbeek, F., and van de Water, B. (2013) Annexin A2 depletion delays EGFR endocytic trafficking via cofilin activation and enhances EGFR signaling and metastasis formation. *Oncogene* 10.1038/onc.2013.219
27. Gerke, V., and Moss, S. E. (2002) Annexins: from structure to function. *Physiol. Rev.* **82,** 331–371
28. Raynal, P., and Pollard, H. B. (1994) Annexins: the problem of assessing the biological role for a gene family of multifunctional calcium- and phospholipid-binding proteins. *Biochim. Biophys. Acta* **1197,** 63–93
29. Rescher, U., and Gerke, V. (2004) Annexins–Unique membrane binding proteins with diverse functions. *J. Cell Sci.* **117,** 2631–2639
30. Tamma, G., Procino, G., Mola, M. G., Svelto, M., and Valenti, G. (2008) Functional involvement of annexin-2 in cAMP-induced AQP2 trafficking. *Pflugers Arch.* **456,** 729–736
31. Dihazi, H., Asif, A. R., Agarwal, N. K., Doncheva, Y., and Müller, G. A. (2005) Proteomic analysis of cellular response to osmotic stress in thick ascending limb of Henle's loop (TALH) cells. *Mol Cell. Proteomics* **4,** 1445–1458
32. Yu, M. J., Miller, R. L., Uawithya, P., Rinschen, M. M., Khositseth, S., Braucht, D. W., Chou, C. L., Pisitkun, T., Nelson, R. D., and Knepper, M. A. (2009) Systems–Level analysis of cell-specific AQP2 gene expression in renal collecting duct. *Proc. Natl. Acad. Sci. U.S.A.* **106,** 2441–2446
33. Meade, P., Hoover, R. S., Plata, C., Vázquez, N., Bobadilla, N. A., Gamba, G., and Hebert, S. C. (2003) cAMP-dependent activation of the renal-specific Na^+-K^+-$2Cl^-$ cotransporter is mediated by regulation of cotransporter trafficking. *Am. J. Physiol. Renal Physiol.* **284,** F1145–F1154
34. Ortiz, P. A. (2006) cAMP increases surface expression of NKCC2 in rat thick ascending limbs: Role of VAMP. *Am. J. Physiol. Renal Physiol.* **290,** F608–F616
35. Drücker, P., Pejic, M., Galla, H. J., and Gerke, V. (2013) Lipid segregation and membrane budding induced by the peripheral membrane binding protein annexin A2. *J. Biol. Chem.* **288,** 24764–24776
36. Rescher, U., and Gerke, V. (2008) S100A10/p11: family, friends, and functions. *Pflugers Arch.* **455,** 575–582
37. Schmitt, R., Klussmann, E., Kahl, T., Ellison, D. H., and Bachmann, S. (2003) Renal expression of sodium transporters and aquaporin-2 in hypothyroid rats. *Am. J. Physiol. Renal Physiol.* **284,** F1097–F1104
38. Yang, T., Park, J. M., Arend, L., Huang, Y., Topaloglu, R., Pasumarthy, A., Praetorius, H., Spring, K., Briggs, J. P., and Schnermann, J. (2000) Low chloride stimulation of prostaglandin E2 release and cyclooxygenase-2 expression in a mouse macula densa cell line. *J. Biol. Chem.* **275,** 37922–37929
39. Eng, B., Mukhopadhyay, S., Vio, C. P., Pedraza, P. L., Hao, S., Battula, S., Sehgal, P. B., McGiff, J. C., and Ferreri, N. R. (2007) Characterization of a long-term rat mTAL cell line. *Am. J. Physiol. Renal Physiol.* **293,** F1413–F1422
40. Cheng, H. F., Wang, J. L., Zhang, M. Z., McKanna, J. A., and Harris, R. C. (2000) Role of p38 in the regulation of renal cortical cyclooxygenase-2 expression by extracellular chloride. *J. Clin. Invest.* **106,** 681–688
41. Welker, P., Geist, B., Frühauf, J. H., Salanova, M., Groneberg, D. A., Krause, E., and Bachmann, S. (2007) Role of lipid rafts in membrane delivery of renal epithelial Na^+-K^+-ATPase, thick ascending limb. *Am. J. Physiol. Regul. Integr. Comp. Physiol.* **292,** R1328–R1337
42. Mutig, K., Paliege, A., Kahl, T., Jöns, T., Müller-Esterl, W., and Bachmann, S. (2007) Vasopressin V2 receptor expression along rat, mouse, and human renal epithelia with focus on TAL. *Am. J. Physiol. Renal Physiol.* **293,** F1166–F1177
43. Hoyer, J. R. (1980) Tubulointerstitial immune complex nephritis in rats immunized with Tamm-Horsfall protein. *Kidney Int.* **17,** 284–292
44. Stelzl, U., Worm, U., Lalowski, M., Haenig, C., Brembeck, F. H., Goehler, H., Stroedicke, M., Zenkner, M., Schoenherr, A., Koeppen, S., Timm, J., Mintzlaff, S., Abraham, C., Bock, N., Kietzmann, S., Goedde, A., Toksöz, E., Droege, A., Krobitsch, S., Korn, B., Birchmeier, W., Lehrach, H., and Wanker, E. E. (2005) A human protein-protein interaction network: A resource for annotating the proteome. *Cell* **122,** 957–968
45. Wanker, E. E., Rovira, C., Scherzinger, E., Hasenbank, R., Wälter, S., Tait, D., Colicelli, J., and Lehrach, H. (1997) HIP-I: A huntingtin interacting protein isolated by the yeast two-hybrid system. *Hum. Mol. Genet.* **6,** 487–495
46. Suter, B., and Wanker, E. E. (2012) The investigation of binary PPIs with the classical yeast two-hybrid (Y2H) approach, Y2H variants, and other *in vivo* methods for PPI mapping. *Methods Mol. Biol.* **812,** v–vi
47. Chabardès-Garonne, D., Mejéan, A., Aude, J. C., Cheval, L., Di Stefano, A., Gaillard, M. C., Imbert-Teboul, M., Wittner, M., Balian, C., Anthouard, V., Robert, C., Ségurens, B., Wincker, P., Weissenbach, J., Doucet, A., and Elalouf, J. M. (2003) A panoramic view of gene expression in the human kidney. *Proc. Natl. Acad. Sci. U.S.A.* **100,** 13710–13715
48. Flicek, P., Amode, M. R., Barrell, D., Beal, K., Brent, S., Carvalho-Silva, D., Clapham, P., Coates, G., Fairley, S., Fitzgerald, S., Gil, L., Gordon, L., Hendrix, M., Hourlier, T., Johnson, N., Kähäri, A. K., Keefe, D., Keenan, S., Kinsella, R., Komorowska, M., Koscielny, G., Kulesha, E., Larsson, P., Longden, I., McLaren, W., Muffato, M., Overduin, B., Pignatelli, M., Pritchard, B., Riat, H. S., Ritchie, G. R., Ruffier, M., Schuster, M., Sobral, D., Tang, Y. A., Taylor, K., Trevanion, S., Vandrovcova, J., White, S., Wilson, M., Wilder, S. P., Aken, B. L., Birney, E., Cunningham, F., Dunham, I., Durbin, R., Fernández-Suarez, X. M., Harrow, J., Herrero, J., Hubbard, T. J., Parker, A., Proctor, G., Spudich, G., Vogel, J., Yates, A., Zadissa, A., and Searle, S. M. (2012) Ensembl 2012. *Nucleic Acids Res.* **40,** D84–D90
49. Guberman, J. M., Ai, J., Arnaiz, O., Baran, J., Blake, A., Baldock, R., Chelala, C., Croft, D., Cros, A., Cutts, R. J., Di Génova, A., Forbes, S., Fujisawa, T., Gadaleta, E., Goodstein, D. M., Gundem, G., Haggarty, B., Haider, S., Hall, M., Harris, T., Haw, R., Hu, S., Hubbard, S., Hsu, J., Iyer, V., Jones, P., Katayama, T., Kinsella, R., Kong, L., Lawson, D., Liang, Y., Lopez-Bigas, N., Luo, J., Lush, M., Mason, J., Moreews, F., Ndegwa, N., Oakley, D., Perez-Llamas, C., Primig, M., Rivkin, E., Rosanoff, S., Shepherd, R., Simon, R., Skarnes, B., Smedley, D., Sperling, L., Spooner, W., Stevenson, P., Stone, K., Teague, J., Wang, J., Whitty, B., Wong, D. T., Wong-Erasmus, M., Yao, L., Youens-Clark, K., Yung, C., Zhang, J., and Kasprzyk, A. (2011) BioMart Central Portal: an open database network for the biological community. *Database* 2011, bar041
50. Paliege, A., Roeschel, T., Neymeyer, H., Seidel, S., Kahl, T., Daigeler, A. L., Mutig, K., Mrowka, R., Ferreri, N. R., Wilson, B. S., Himmerkus, N., Bleich, M., and Bachmann, S. (2012) Group VIA phospholipase A2 is a target for vasopressin signaling in the thick ascending limb. *Am. J. Physiol. Renal Physiol.* **302,** F865–F874
51. Wilson, B. S., Steinberg, S. L., Liederman, K., Pfeiffer, J. R., Surviladze, Z., Zhang, J., Samelson, L. E., Yang, L. H., Kotula, P. G., and Oliver, J. M. (2004) Markers for detergent-resistant lipid rafts occupy distinct and dynamic domains in native membranes. *Mol. Biol. Cell* **15,** 2580–2592
52. Livak, K. J., and Schmittgen, T. D. (2001) Analysis of relative gene expression data using real-time quantitative PCR and the $2(-\Delta\Delta C(T))$ Method. *Methods* **25,** 402–408
53. Gerke, V., and Moss, S. E. (1997) Annexins and membrane dynamics. *Biochim. Biophys. Acta* **1357,** 129–154
54. Grewal, T., and Enrich, C. (2009) Annexins–Modulators of EGF receptor signalling and trafficking. *Cell. Signal.* **21,** 847–858
55. van de Graaf, S. F., Hoenderop, J. G., and Bindels, R. J. (2006) Regulation of TRPV5 and TRPV6 by associated proteins. *Am. J. Physiol. Renal Physiol.*

290, F1295–F1302
56. Gerke, V., and Weber, K. (1985) The regulatory chain in the p36-kDa substrate complex of viral tyrosine-specific protein kinases is related in sequence to the S-100 protein of glial cells. *EMBO J.* **4,** 2917–2920
57. Glenney, J. R., Jr., and Tack, B. F. (1985) Amino-terminal sequence of p36 and associated p10: identification of the site of tyrosine phosphorylation and homology with S-100. *Proc. Natl. Acad. Sci. U.S.A.* **82,** 7884–7888
58. Krager, K. J., Sarkar, M., Twait, E. C., Lill, N. L., and Koland, J. G. (2012) A novel biotinylated lipid raft reporter for electron microscopic imaging of plasma membrane microdomains. *J. Lipid Res.* **53,** 2214–2225
59. Bickel, P. E., Scherer, P. E., Schnitzer, J. E., Oh, P., Lisanti, M. P., and Lodish, H. F. (1997) Flotillin and epidermal surface antigen define a new family of caveolae-associated integral membrane proteins. *J. Biol. Chem.* **272,** 13793–13802
60. Santamaría, A., Castellanos, E., Gómez, V., Benedit, P., Renau-Piqueras, J., Morote, J., Reventós, J., Thomson, T. M., and Paciucci, R. (2005) PTOV1 enables the nuclear translocation and mitogenic activity of flotillin-1, a major protein of lipid rafts. *Mol. Cell. Biol.* **25,** 1900–1911
61. Harder, T., Scheiffele, P., Verkade, P., and Simons, K. (1998) Lipid domain structure of the plasma membrane revealed by patching of membrane components. *J. Cell Biol.* **141,** 929–942
62. Magee, A. I., and Parmryd, I. (2003) Detergent-resistant membranes and the protein composition of lipid rafts. *Genome Biol.* **4,** 234
63. Cavallone, D., Malagolini, N., and Serafini-Cessi, F. (2001) Mechanism of release of urinary Tamm-Horsfall glycoprotein from the kidney GPI-anchored counterpart. *Biochem. Biophys. Res. Commun.* **280,** 110–114
64. Johnstone, S. A., Hubaishy, I., and Waisman, D. M. (1992) Phosphorylation of annexin II tetramer by protein kinase C inhibits aggregation of lipid vesicles by the protein. *J. Biol. Chem.* **267,** 25976–25981
65. Jost, M., and Gerke, V. (1996) Mapping of a regulatory important site for protein kinase C phosphorylation in the N-terminal domain of annexin II. *Biochim. Biophys. Acta* **1313,** 283–289
66. Borthwick, L. A., McGaw, J., Conner, G., Taylor, C. J., Gerke, V., Mehta, A., Robson, L., and Muimo, R. (2007) The formation of the cAMP/protein kinase A-dependent annexin 2-S100A10 complex with cystic fibrosis conductance regulator protein (CFTR) regulates CFTR channel function. *Mol. Biol. Cell* **18,** 3388–3397
67. Mazzone, A., Tietz, P., Jefferson, J., Pagano, R., and LaRusso, N. F. (2006) Isolation and characterization of lipid microdomains from apical and basolateral plasma membranes of rat hepatocytes. *Hepatology* **43,** 287–296
68. Ayala-Sanmartin, J., Henry, J. P., and Pradel, L. A. (2001) Cholesterol regulates membrane binding and aggregation by annexin 2 at submicromolar Ca^{2+} concentration. *Biochim. Biophys. Acta* **1510,** 18–28
69. Rescher, U., Ruhe, D., Ludwig, C., Zobiack, N., and Gerke, V. (2004) Annexin 2 is a phosphatidylinositol (4,5)-bisphosphate binding protein recruited to actin assembly sites at cellular membranes. *J. Cell Sci.* **117,** 3473–3480
70. Chasserot-Golaz, S., Vitale, N., Umbrecht-Jenck, E., Knight, D., Gerke, V., and Bader, M. F. (2005) Annexin 2 promotes the formation of lipid microdomains required for calcium-regulated exocytosis of dense-core vesicles. *Mol. Biol. Cell* **16,** 1108–1119
71. Zaarour, N., Demaretz, S., Defontaine, N., Mordasini, D., and Laghmani, K. (2009) A highly conserved motif at the COOH terminus dictates endoplasmic reticulum exit and cell surface expression of NKCC2. *J. Biol. Chem.* **284,** 21752–21764
72. Zaarour, N., Defontaine, N., Demaretz, S., Azroyan, A., Cheval, L., and Laghmani, K. (2011) Secretory carrier membrane protein 2 regulates exocytic insertion of NKCC2 into the cell membrane. *J. Biol. Chem.* **286,** 9489–9502
73. Zaarour, N., Demaretz, S., Defontaine, N., Zhu, Y., and Laghmani, K. (2012) Multiple evolutionarily conserved di-leucine like motifs in the carboxyl terminus control the anterograde trafficking of NKCC2. *J. Biol. Chem.* **287,** 42642–42653
74. Saritas, T., Borschewski, A., McCormick, J. A., Paliege, A., Dathe, C., Uchida, S., Terker, A., Himmerkus, N., Bleich, M., Demaretz, S., Laghmani, K., Delpire, E., Ellison, D. H., Bachmann, S., and Mutig, K. (2013) SPAK differentially mediates vasopressin effects on sodium cotransporters. *J. Am. Soc. Nephrol.* **24,** 407–418
75. McCormick, J. A., Mutig, K., Nelson, J. H., Saritas, T., Hoorn, E. J., Yang, C. L., Rogers, S., Curry, J., Delpire, E., Bachmann, S., and Ellison, D. H. (2011) A SPAK isoform switch modulates renal salt transport and blood pressure. *Cell Metab.* **14,** 352–364
76. Reiche, J., Theilig, F., Rafiqi, F. H., Carlo, A. S., Militz, D., Mutig, K., Todiras, M., Christensen, E. I., Ellison, D. H., Bader, M., Nykjaer, A., Bachmann, S., Alessi, D., and Willnow, T. E. (2010) SORLA/SORL1 functionally interacts with SPAK to control renal activation of Na^+-K^+-$2Cl^-$ cotransporter 2. *Mol. Cell. Biol.* **30,** 3027–3037
77. Urbanska, A., Sadowski, L., Kalaidzidis, Y., and Miaczynska, M. (2011) Biochemical characterization of APPL endosomes: The role of annexin A2 in APPL membrane recruitment. *Traffic* **12,** 1227–1241
78. Grieve, A. G., Moss, S. E., and Hayes, M. J. (2012) Annexin A2 at the interface of actin and membrane dynamics: a focus on its roles in endocytosis and cell polarization. *Int. J. Cell Biol.* 2012, 852430
79. Okuse, K., Malik-Hall, M., Baker, M. D., Poon, W. Y., Kong, H., Chao, M. V., and Wood, J. N. (2002) Annexin II light chain regulates sensory neuron-specific sodium channel expression. *Nature* **417,** 653–656
80. Poon, W. Y., Malik-Hall, M., Wood, J. N., and Okuse, K. (2004) Identification of binding domains in the sodium channel Na(V)1.8 intracellular N-terminal region and annexin II light chain p11. *FEBS Lett.* **558,** 114–118
81. Mayer, G., Poirier, S., and Seidah, N. G. (2008) Annexin A2 is a C-terminal PCSK9-binding protein that regulates endogenous low density lipoprotein receptor levels. *J. Biol. Chem.* **283,** 31791–31801
82. Fenton, R. A., and Moeller, H. B. (2008) Recent discoveries in vasopressin-regulated aquaporin-2 trafficking. *Prog. Brain Res.* **170,** 571–579
83. Moeller, H. B., and Fenton, R. A. (2012) Cell biology of vasopressin-regulated aquaporin-2 trafficking. *Pflugers Arch.* **464,** 133–144
84. Menke, M., Ross, M., Gerke, V., and Steinem, C. (2004) The molecular arrangement of membrane-bound annexin A2-S100A10 tetramer as revealed by scanning force microscopy. *Chembiochem* **5,** 1003–1006
85. Menke, M., Gerke, V., and Steinem, C. (2005) Phosphatidylserine membrane domain clustering induced by annexin A2/S100A10 heterotetramer. *Biochemistry* **44,** 15296–15303
86. Schmitt, J. M., and Stork, P. J. (2002) PKA phosphorylation of Src mediates cAMP's inhibition of cell growth via Rap1. *Mol. Cell* **9,** 85–94
87. Borthwick, L. A., Riemen, C., Goddard, C., Colledge, W. H., Mehta, A., Gerke, V., and Muimo, R. (2008) Defective formation of PKA/CnA-dependent annexin 2-S100A10/CFTR complex in ΔF508 cystic fibrosis cells. *Cell. Signal.* **20,** 1073–1083
88. Brandherm, I., Disse, J., Zeuschner, D., and Gerke, V. (2013) cAMP-induced secretion of endothelial von Willebrand factor is regulated by a phosphorylation/dephosphorylation switch in annexin A2. *Blood* **122,** 1042–1051
89. Hebert, S. C., Friedman, P. A., and Andreoli, T. E. (1984) Effects of antidiuretic hormone on cellular conductive pathways in mouse medullary thick ascending limbs of Henle: I. ADH increases transcellular conductance pathways. *J. Membr. Biol.* **80,** 201–219